



Degradation Processes of Two Compound Layers on Nitrided Surfaces During the Wear Test by “Block on Hot Al Cylinder”

M. LAMUT,¹ J. BURJA,¹ M. TERČELJ,¹ G. KUGLER,¹
and D. BOMBAČ^{1,2}

1.—Faculty of Natural Science and Technology, Department of Materials and Metallurgy, University of Ljubljana, Aškerčeva cesta 12, 1000 Ljubljana, Slovenia.
2.—e-mail: david.bombac@ntf.uni-lj.si

The results obtained in the study help to explain the degradation process of the nitrided steel compound layer. Compound layers with different properties on gas-nitrided H10 tool steel blocks were tested for wear with “block on hot Al cylinder”. Degradation processes were observed on both compound layers with different properties and at three contact pressures. In order to observe the degradation processes in the compound layers, the wear tests were interrupted at various fixed time intervals and the resulting changes were closely monitored. The comprehensive analysis highlighted the complexity of the degradation process in the compound layers and emphasized the existence of complex relationships between the above-mentioned parameters. The reaction of the nitrided steel surface with hot Al is more pronounced in areas with lower contact pressure, while adhesive removal and furrow formation are pronounced in areas with low and medium contact pressure. This process begins with a sufficient density of the areas where islands of adhesive removal are located, their enlargement during the test, the breaking up of the walls between them, and finally the removal of the compound layer in the sliding direction, which appears as furrowing in the final phase of wear.

INTRODUCTION

Extending the service life of tools for hot Al extrusion is an important factor in improving the economics of the production process. This can be achieved by improving the die design, reducing the contact pressure on the die-bearing surfaces, proper selection of deformation parameters, improving the properties of die materials (AISI H10, H11, H13), etc., and increasing the wear resistance of the bearing surfaces by gas, ion, and salt bath nitriding,^{1–5} as well as CVD and PVD treatments.^{6–13} The gas nitriding process is also suitable for deep and narrow gaps in the bearing surfaces of tools for the extrusion of complex profiles. Due to the complexity of the extruded profiles, most of the bearing surfaces of extrusion dies form narrow and deep crevices (gaps), so research on the wear progress of different

gas-nitrided surfaces is important.^{1–3} Several studies have been carried out on the degradation of the compound layer under different loading conditions,^{13–16} but the degradation pathways, particularly with regard to the properties of the compound layer and the contact pressure, have not yet been fully clarified.

The tribological system in hot extrusion of aluminum is very demanding, as it takes place at temperatures close to the melting point of the extruded Al alloys (above 600°C). The contact pressures on the bearing surface usually vary around the circumference of the die-bearing surface and decrease towards the exit edge, while the exit speeds of the extruded products are in the range of 5–100 m/min. The contact pressure and distribution on the die support surface are influenced by the extrusion ratio, temperature, deformation rate, die design, etc.^{1–3,6–9,17,18}

During gas nitriding of die steels, in general, two different microstructures can form on the die-bearing surfaces: (1) the microstructure with a

“composite layer” on top of the surface with a diffusion layer underneath, and (2) the diffusion layer alone. The compound layer usually consists of a brittle γ' -phase (γ' -Fe₄N), an ϵ -phase (ϵ -Fe₂₋₃N), or a mixture (heterogeneous phase mixture) ($\epsilon + \gamma'$).^{1-5,14-16,19-21} The phase structure of the compound layer, i.e., its composition (two-phase or single-phase, or its ratio), has a significant impact on the brittleness and consequently on the performance. For example, a single-phase compound layer, Fe₄N, is less brittle than a single-phase, Fe₂₋₃N, while a mixed-phase layer again has increased brittleness. Furthermore, the quality of the compound layer depends on the presence of porosity and nitrides. The wear resistance should therefore be considered as a function of the properties of the diffusion layer, i.e., its hardness profile, diffusion depth, and microstructure, and as a function of temperature, and mechanical, chemical, and tribological loading. Reduced quality can be the result of an unsuitable initial microstructure of the tool steel used, unsuitable prior preparation of the bearing surface, and the use of unsuitable nitriding parameters (nitriding potential, temperature, time, etc.), and so on.^{1-5,14-16,22-28} The compound layer usually improves corrosion, erosion, and thermal fatigue resistance.^{1,29-39} and, in special cases (relatively low contact pressures), wear resistance as its desired properties which are related to tribological loads. In two-body tribology systems, the contact, i.e., the contact pressure, as well as the temperature, have a decisive influence on the prevailing wear mechanisms and, consequently, on the wear progress.³⁸⁻⁴¹ It is assumed that complex wear behavior also prevails in the tribological system “soft and heated Al against hard (nitrided) mating body”, since bonding takes place between both elements. Although the wear behavior of nitrided tools has not been fully elucidated in studies,^{1,17,21,35-39,42-47} further experimental results to reveal the complexity are desirable. Degradation of the compound layer was studied in several investigations which were predominately focused on specific load problems, e.g., contact rolling, sliding wear, thermal fatigue behavior, etc., and in relation to the characteristics of the nitrided layer.^{1-5,13-16,24,35-39,47-61} Wear mechanisms, such as adhesion, abrasion, chemical reactions, and cracking, take place.

Wang et al.¹⁴ and Wang et al.⁴⁶ considered that characterizing the relationships between the microstructural features of the nitrided layers, the loads, and the wear behavior was crucial to ensure stable operation of the nitrided components under different conditions. The different service lives of Al extrusion dies, even when extruding very similar or the same profiles, can be attributed to both the occurrence of different contact pressures along the bearing surface and the variety of quality of microstructures obtained on the nitride layers, i.e., their different local properties. Thus, the

characteristics of the microstructure of the nitrided layer on the bearing surface, the prevailing contact pressure, and the temperature are relevant parameters in the operation time of dies for Al hot extrusion, but the complexity of their relationship has not been sufficiently explained, which could be due to the approximation to the real conditions prevailing in the real Al hot extrusion process.

Therefore, further explanations of the relationships between the following parameters in the tribological system during Al hot extrusion, i.e., the degradation processes, the contact pressures, and the properties of the compound layer, are essential for further improving the applicability of nitrided dies (in this case made of AISI H10). This can be shown by the results for tracking the degradation process of selected nitrided layers with their different properties. For this purpose, the laboratory wear test “block on hot Al cylinder” was used to investigate the above-mentioned relationships. Different degradation paths depending on the contact pressures and the properties of the nitrided layers were found, and explanations for this behavior have been given. The obtained results serve as a contribution to the explanation of the degradation progress of the compound layer.

EXPERIMENTAL

Materials and Nitriding

In order to show the degradation processes of compound layers on the tested nitrided samples, the test stand “block on hot Al cylinder” (Fig. 1a) was used for wear tests with the test conditions given in Table I. A rotating cylinder with dimensions $\Phi 146 \text{ mm} \times 35 \text{ mm}$ was made of AA6063 (0.5%Mg, 0.5%Si, 0.19%Fe, 0.05%Mn, balance Al) and represents an extruded Al profile from a tribological point of view. Four nitrided blocks with dimensions $30 \text{ mm} \times 30 \text{ mm} \times 20 \text{ mm}^3$ were made of H10 tool steel and tested for wear. The chemical composition of the H10 tool steel used was (in wt.%): 0.33%C, 0.30%Si, 0.38%Mn, 3.0%Cr, 2.80%Mo, 0.45%V, and balance Fe.

Blocks were gas-nitrided and the microstructures as well as the nitriding depths were similar to gas-nitrided industrial extrusion dies. After gas nitriding, the blocks were also subjected to an oxidation treatment. Gas nitriding and oxidation were carried out in industrial conditions where reliable process parameters could not be recorded.

Wear Testing and Test Conditions

The wear test involves a steel block with a nitrided surface being pressed against a rotating cylinder. The Al cylinder, firmly inserted between two copper and steel discs, was inductively heated to the prescribed surface temperature of over 600°C at the outer surface of cylinder. That temperature is close to the melting point of Al, which makes it possible to establish the tribological conditions that

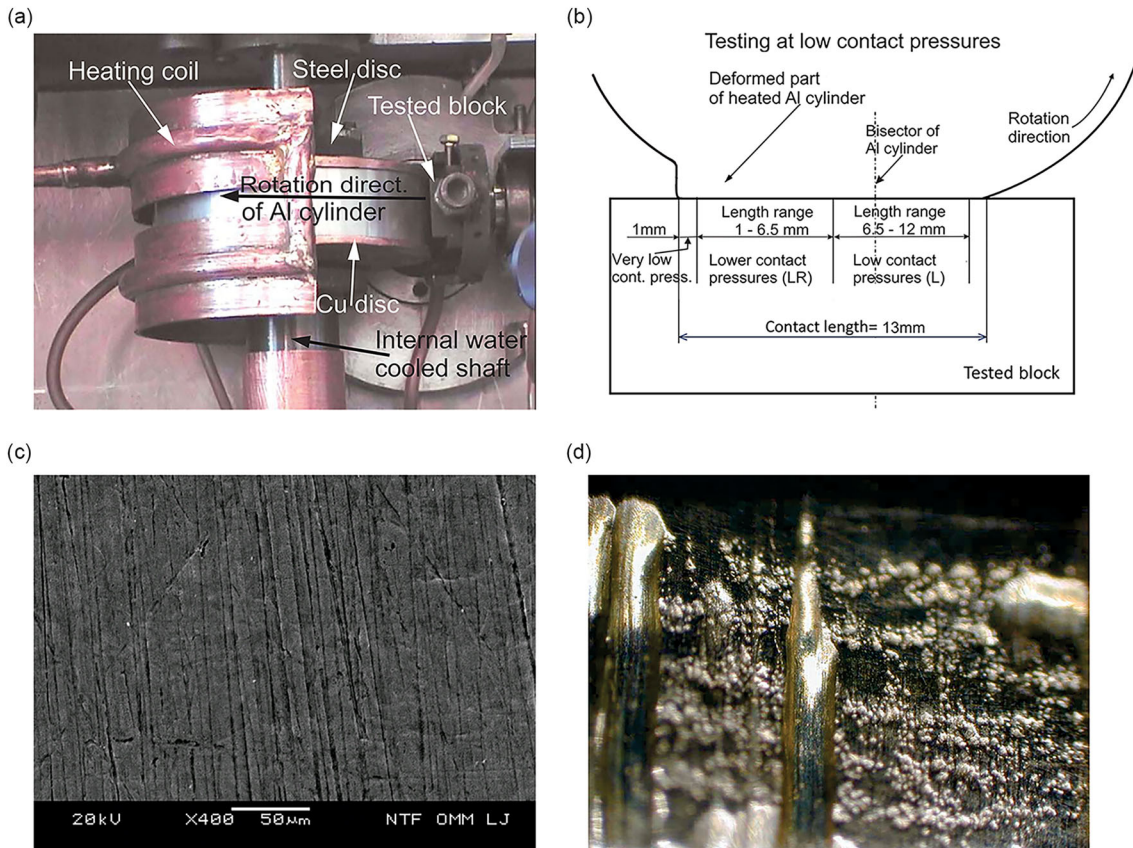


Fig. 1. (a) "Block on hot Al cylinder" wear test rig and (b) sketch showing the different areas in the low contact pressure test with a established length of 13 mm (conditional division of the contact length into two areas), (c) typical appearance of the initial surface of the tested nitrided blocks, and (d) the appearance of the furrows on the bearing surface of the industrial dies.

Table I. Wear test conditions

	Block 1	Block 2	Block 3	Block 4
Assessed contact temp. (°C)	> 600	> 600	> 600	> 600
Established cont. length (mm)	13	10	13	10
Test contact pressure	LR, L	M	LR, L	M
Time of interrupt. (min)	30, 60, 120	30, 60, 120	30, 60, 120	30, 60, 120
Time of wear observation (min)	(LR) 120 (L) 30, 60, 120	(M) 30, 60, 120	(LR) 120 (L) 30, 60, 120	(M) 30, 60, 120
Sliding velocity (m/s)	0.5	0.5	0.5	0.5

LR lower contact pressure, L low contact pressure, M medium contact pressure.

prevail on the die-bearing surface during the industrial Al hot extrusion process. The temperature was measured and controlled by a point pyrometer pointed at the Cu disc. A normal force of 1920 N and a relative sliding speed of 0.5 m/s between the Al cylinder and the tested blocks were used. The wear tests were carried out at two different contact lengths (13 mm and 10 mm). The production of

different contact lengths between the heated Al cylinder and the nitrided blocks was achieved by different temperature gradients as a consequence of changing the ratio of the heat supply in the radial direction to the Al cylinder; (1) from the outside by heating via a heating coil, and (2) from the inside by heating via steel discs, whereby two different diameters were used depending on the contact length

(Fig. 1a). Different intensities of inductive heating of the Al cylinder led to different temperature gradients in the radial depth of the cylinder, which consequently influenced the contact lengths that occurred in the contact (Fig. 1b) and enabled tests with different contact pressures at approximately the same external temperature of the cylinder. It should be noted that the frictional work between the Al cylinder and the tested blocks, as well as the different intensity of the water flow in the internally cooled shaft, also influenced the radial temperature gradients in the Al cylinder. In this way, the contact lengths of 13 mm and 10 mm were established, whereby the determined contact length of approximately 13 mm (Fig. 1b) was considered as a test at low (L) contact pressure, while the established contact length of approximately 10 mm was considered as a test at medium (M) contact pressure. Furthermore, a difference in the wear behavior along the contact length was observed at the determined contact length of 13 mm. The difference in wear pattern was attributed to the distribution of contact pressure along the contact length which was not uniform (continuous changes in contact pressure). Consequently, the contact length was conditionally divided into two additional areas, although it is difficult to make a clear distinction between them, as similar wear behavior was observed on both sides near the fixed limit.

Thus, the first area, i.e., the area in the contact length range of 1–6.5 mm, was conditionally considered a lower contact pressure test (LR), while the second area, i.e., the area in the length range of 6.5–12 mm, was conditionally considered a low contact pressure test (L) (see Fig. 1b). After 2 h of testing, the first tribologically stressed area mentioned above (length range 1–6.5 mm) was also observed. In general, with a fixed contact length of 13 mm, this allowed testing with an average contact pressure value of about 5 MPa. With regard to the continuous change of contact pressures in Fig. 1b, testing at low (L) contact pressure therefore took place above approximately 5 MPa, while testing at lower (LR) contact pressure took place below approximately 5 MPa.

At the established contact length of 10 mm, the average value of the contact pressure was approximately 6.5 MPa, which is considered as testing at medium (M) contact pressure, while the results were observed within the length of 6 mm, i.e., in the range of 2–8 mm of the established contact length (10 mm). The test conditions are shown in Table I. Blocks 1 and 3 were tested at lower (LR) and low (L) contact pressures (see Fig. 1b), while blocks 2 and 4 were tested at medium (M) contact pressures. Figure 1c shows a typical appearance of the initial surface of the tested blocks, with the average roughness R_a being $0.21 \mu\text{m}$.

To prevent oxidation of the Al, an inert atmosphere was created in the test chamber by a flow of argon gas. The wear tests were interrupted after

30 min, 60 min, and 120 min in the inert atmosphere and the progress of degradation on the tested surface was analyzed. The Al adhering to the tested blocks was removed in NaOH solution in order to be able to observe the wear progress on the tribologically loaded surfaces after each test sequence. Progress of the wear on the nitrided blocks was focused on the areas of the tested surface where the sequence of degradation processes could be observed. For the description of the degradation progress, the times of occurrence of the degradation stages typical for the compound and diffusion layers are relevant, i.e., the temporal occurrence of partial adhesion detachment (islands), crack formation, fragmentary detachment, detachment due to reactions with hot Al, detachment oriented in the sliding direction, as well as furrow formation in the sliding direction, etc. It is worth mentioning that the onset of furrow formation on the bearing surface of the extrusion tools, which leads to a rapid decrease in the surface quality of extruded profiles and usually requires repeated grinding of the surface and a nitriding cycle of the tool used, is of particular importance (see Fig. 1d). In this way, a better understanding of the relationships between selected features of the microstructure of the nitrided samples, the test contact pressure used, and the wear processes can be made possible.

At this point, it should be emphasized that the observation of degradation was not carried out at the same points of the tested blocks, i.e., the time of observation was fixed, and relevant processes related to progress could be lost in this way, as they may occur earlier or later in relation to the fixed time of observation. Therefore, in order to track the relevant progress of the degradation, different locations on the tested surface were selected for observation, through the images of which the continuation of the progress can be revealed.

Characterization of Microstructure and Wear Progress

The following equipment was used to characterize the nitrided layer on the tested blocks. Vickers microhardness measurements were carried out with a Fischerscope H100C using a 100-g weight, the microstructures were imaged with an OLYMPUS BX60M light microscope (nital etchant was used) and X-ray diffraction (XRD) studies of the compound layer were carried out with a Siemens Analytical D5000 diffractometer with a Cu anode where 2θ was between 15° and 90° . The degradation progress of the nitrided layers was identified by scanning electron microscopy (SEM) and backscatter electron microscopy (BSE) using JEOL JSM 5610 and ZEISS CrossBeam 550 microscopes, respectively. The working distances were 9–12 mm, and the accelerating voltages were 15 kV and 20 kV.

RESULTS AND DISCUSSION

Initial Microstructures and XRD of Tested Blocks

The microstructure of the base material consists of a tempered martensitic matrix, with carbonitrides (chromium and molybdenum). The hardness of the base material was measured to be 516 HV. The nitrided surfaces of all four tested blocks consisted of a compound layer covered by a thin oxide layer. XRD revealed predominately the presence of the ϵ phase in all the tested compound layers of blocks. The main characteristics of the nitrided layer are given in Table II. The microstructures of the compound layer of the nitrided blocks are shown in Fig. 2a, b, c, and d for blocks 1 and 2 and in Fig. 2e and f for blocks 3 and 4. Figure 2a, b, and e indicate that the formation of the hexagonal ϵ iron nitride layer progresses along crystal slip planes. Interestingly, molybdenum carbonitrides are still present in the ϵ compound layer, seen as white particles in the BSE SEM images in Fig. 2a, b, and e. These carbonitrides present a discontinuity in the ϵ layer. Furthermore, energy-dispersive X-ray spectroscopy (EDS) linear analysis of the carbonitrides was carried out (see Table III), and the microhardness profiles are given in Fig. 3 for all the tested blocks. Carbonitrides are based on Mo (see Fig. 2c), V, and Cr (see Table III). Figure 2a and b shows that the compound layer thickness on blocks 1 and 2 ranged from 6 μm to 8 μm , while the weak oxidation depth was ca 1.5 μm (see Fig. 2c). Almost no nitrides on the grain boundaries of the diffusion layer were observed. The nitriding depth was approximately 110 μm (see Fig. 3), and the microhardness reached a maximum value of 1060 HV0.1.

The compound layer of nitrided blocks 3 and 4 was slightly thinner and ranged from 5 μm to 7 μm , including Mo, V, and Cr carbonitrides (see Fig. 2e and f) with a clear presence of an oxide layer about 1.5 μm thick (see Fig. 2f). The EDS analysis of the oxide layer was inconclusive, showing only a slight variation in O content for blocks 1 and 2 (measured at 2 wt.%) and for blocks 3 and 4 (measured at about 2.5 wt.%). However, EDS elemental mapping showed a more pronounced difference in oxygen

distribution between the oxide and the nitride layer for blocks 3 and 4, such that the oxide layer was more pronounced and had a clearer border (Fig. 2d, e, and f).

The nitriding depth of blocks 3 and 4 was about 90 μm (see Fig. 3), and the compound layer and the presence of the nitrides were visible at the grain boundaries, as shown in Fig. 2e. The maximum value for microhardness was also lower for blocks 3 and 4 compared to blocks 1 and 2 and was about 940 HV0.1. A slightly increased presence of porosity can be seen in the compound layer of blocks 3 and 4 (Fig. 2e) compared to blocks 1 and 2 (Fig. 2a and b), which may indicate a possibly lower quality of the compound layer in blocks 3 and 4. EDS analysis of the carbonitrides at the marked location in Fig. 2b and e was carried out. The chemical composition of the carbonitrides in blocks 3 and 4 was found to be similar to that of blocks 1 and 2, i.e., the carbonitrides are based on molybdenum with measured content in the range of about 15–28 wt%.

Wear Progress at Low (L) Contact Pressure

Wear at low contact pressure was tested on blocks 1 and 3 and the progress of degradation is described below. It should be emphasized here that the figures presented and discussed describe the progress of the degradation process to reconstruct the degradation process and not necessarily the most severe wear.

Block 1

The compound layer in blocks 1 and 2 has less porosity, diffusion depth is deeper from the surface, and measured hardness profile harder compared to blocks 3 and 4. This indicates potentially better wear properties or higher degradation resistance. The main wear features that can be observed after 30 min of testing in block 1 are two initial modes (types) of wear of the compound layer. The first is due to the occurrence of small initial cracks in the compound layer and the second mode refers to very small adhesive removal (formation of small islands), without visible initial cracks [see Fig. 4a (SEM) and b (BSE)]. Note that Fig. 4a (SEM) and b (BSE) show

Table II. Main characteristics of tested nitrided blocks

Blocks	1, 2	3, 4
Max. microhardness HV0.1	1060	940
Nitriding depth (μ)	110	90
CL thickness (μm)	6–8	5–7
Presence of oxide layer on top of CL (thickness in μm)	Weak (1)	Emphasized (1,5)
Presence of carbonitrides and porosity in CL	Yes	Yes

CL compound layer.

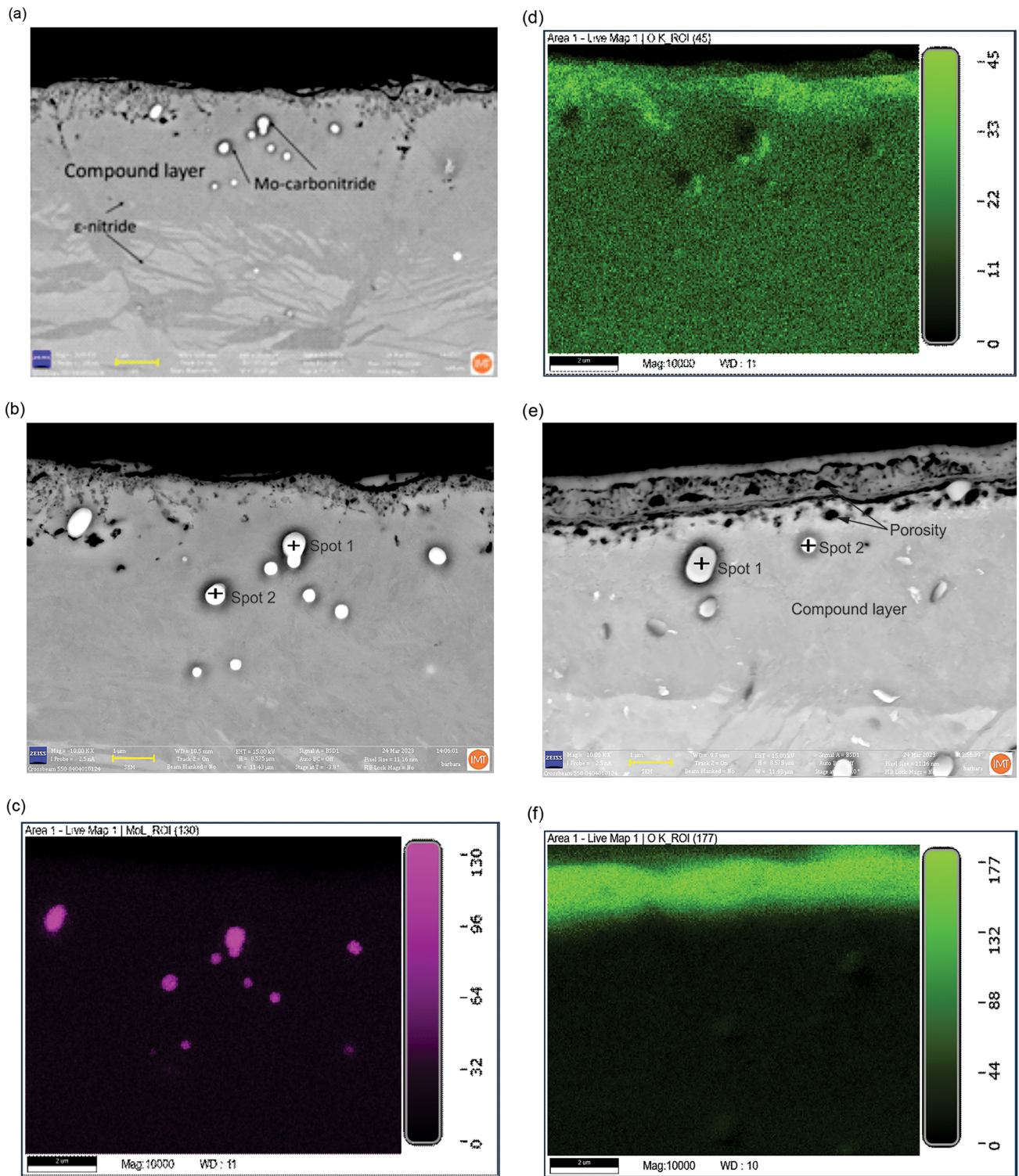


Fig. 2. (a–d) Main features of the compound layers; blocks 1 and 2, and (e, f) blocks 3 and 4; (a, b) microstructure of the compound layer, (c) distribution of Mo in carbonitrides, (d) distribution of oxygen, (e) microstructure of the compound layer of blocks 3 and 4, and (f) distribution of oxygen.

the same spot on the tested surface, confirming the coexistence of both wear modes of the compound layer at this stage of surface degradation progress.

As will be seen more clearly later, both types are related to the presence of a lower density of carbonitrides and porosity in the compound layer.

Table III. Quantitative EDS analysis of blocks 1 and 2 at spots 1 and 2 (Fig. 2b) and blocks 3 and 4 at spots 1 and 2 (Fig. 2e)

	<u>C</u>	<u>N</u>	<u>O</u>	<u>Al</u>	<u>Si</u>	<u>V</u>	<u>Cr</u>	<u>Mn</u>	<u>Fe</u>	<u>Ni</u>	<u>Mo</u>
Spot 1, Fig. 2b	21.1	18.7	5.0	0.1	0.7	1.0	1.8	0.1	32.7	0.1	18.8
Spot 2, Fig. 2b	21.3	19.3	6.0	0.2	1.1	1.2	1.8	0.1	21.3	0.0	27.7
Spot 1, Fig. 2e	20.1	20.9	4.4	0.2	0.9	1.3	1.9	0.1	23.9	0.1	27.0
Spot 2, Fig. 2e	17.3	19.1	5.1	0.1	0.7	1.0	1.9	0.1	38.8	0.1	15.9

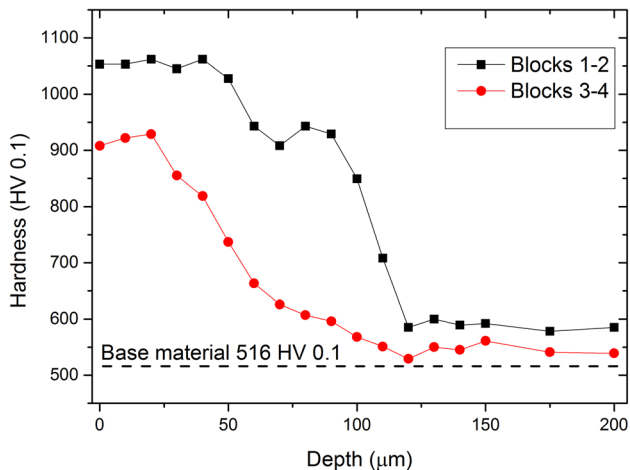


Fig. 3. Microhardness profiles of tested blocks.

Indeed, carbonitrides and porosity were observed in some locations where the compound layer had previously been partially removed, observed as very shallow islets (Fig. 4c with the location for detail A shown in Fig. 4d). The presence of carbonitrides and porosity thus affects the removal of the compound layer, as shear strength decreases and brittleness increases at these locations. In addition, the increased roughness at the sites where the compound layer was initially removed only slightly (at the bottom of the islands) contributes to the increase in adhesion. This leads to a potentially accelerated removal of the fragments at these sites and consequently to a deepening of the islands as the next stage of the compound layer degradation. On the other hand, it is evident from Fig. 4a that the removal or adhesion of the compound layer occurs even without observed porosity at the sites of its partial erosion. This second type of adhesive removal without highlighted initial surface cracking of the compound layer can also be attributed to the strong adhesion between the hot Al and the compound layer. The degradation mode (cracking or adhesion removal) depends on the local density of porosity and carbonitrides, their distribution, and their relation to tribologically loaded surfaces. Cracking occurs when the porosity and carbonitride density are high in the normal direction. With increased density in the direction of frictional stress and at a short distance from the surface, slightly increased adhesive removal may occur. Smaller

adhesive erosion can take place without the presence of porosity and carbonitrides at the erosion site.

EDS analyses were carried out at selected locations, as shown in Fig. 4a. The analyses showed no clear evidence of a chemical reactions between Al and the surface of the bonding layer in the non-removed areas (point 3 in Fig. 4a), no peak for Al (Fig. 4e), and only a small peak for Mg (Al cylinders also contain Mg, cf. Table I). However, on the partly removed area of the compound layer (point 2 in Fig. 4a), hardly visible peaks for Al and Mg can be seen (Fig. 4f), which also indicates a possible reaction of the nitrated surface of the tested block with the hot Al. In addition, highlighted peaks for Al and Mg were obtained at point 1 (i.e., in the microcrack; Fig. 4a), which can be attributed to undissolved Al in the crack. Thus, from these analytical results, it can be inferred that the undamaged surface of the composite layer is probably more wear-resistant to hot Al than the new surface formed by adhesion at the bottom of the islets, which is also rougher. As already mentioned, this accelerates further adhesion in such places, seen as the formation of deeper islands, as described in Fig. 5, can take place. The surface of the compound layer has a lower roughness and a higher nitrogen content.

After 60 min of testing block 1, the degradation process continued and led to an increased crack density in the compound layer as well as an increased number of locations where the adhesive layer detaches down to the diffusion layer (see Fig. 5a) with the location for detail B shown in Fig. 5b for detachment), with the formation of small and deeper islets. A typical image from the lower end of the complete removal of the compound layer is shown in Fig. 5c, where the onset of cracking in the diffusion layer can be observed. As expected, Fig. 5a also shows an increased number of locations where the compound layer was only partially removed, with the visible presence of carbonitrides and porosity at the locations of removal, as well as surface cracking.

Due to the mentioned presence of carbonitrides and porosity in the compound layer, several different types of initial adhesion removal were observed on the tested surface. The first type of removal, called crack propagation in the compound layer,

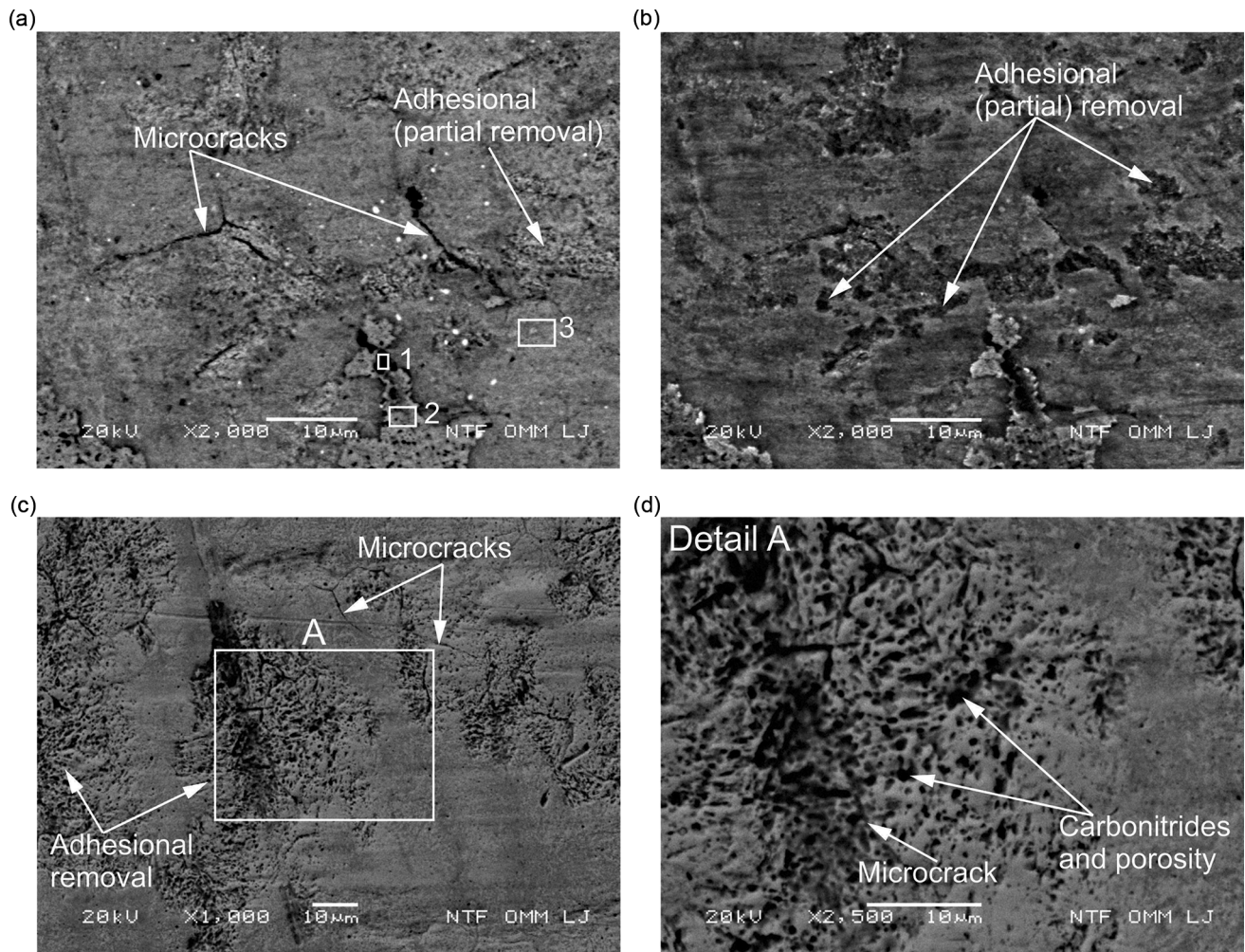


Fig. 4. Main wear characteristics of the compound layer of block 1 after 30 min of testing; areas showing the first and second phase of wear progression: (a) initial surface microcracks (BSE) with locations marked for EDS analysis, (b) initial surface microcracks (SEM), (c) removal of the compound layer around initial cracks (BSE), and (d) detail box A in (c) of removal of the compound layer around cracks with visible porosity (BSE). (e) EDS analysis at location 1 in (a), (f) EDS analysis at location 2 in (a), (g) EDS analysis at location 3 in (a); low contact pressure, sliding direction ←, block 1.

starts at locations where there is a sufficiently high density of carbonitrides and pores locally in the plane from the surface to the diffusion layer. Moreover, carbonitrides are locally distributed near the surface throughout the thickness of the compound layer. Due to the high normal and frictional stresses that occur during Al sliding, the cracks (fracture surface) grow from the surface towards the diffusion layer (in Fig. 5d with an angle of about 45°). The remaining fragments adhere to the top of the second fracture surface of the tested surface indicating that the fragment broke away from their original location just before the 60-min test was interrupted. This provides additional confirmation that this type of detachment is a result of the high frictional stresses that cause the “crumbs” to break away from the compound layer.

The second type of initial detachment of the compound layer can be observed in places (patches)

where there is locally a sufficiently high carbonitride and pore density, closer to the surface of the compound layer and in a predominantly horizontal direction. The appearance of a newly formed surface (see Fig. 5e) indicates that the gradual removal of the compound layer is a consequence of the adhesion between the hot Al and the compound layer. As can be seen from the comparison of Fig. 5d and e, the depth of removal of the compound layer is less in Fig. 5e, but the density of the removed areas is higher. In addition, the slope angle of the newly formed surface is also usually much lower than in the previous case, due to the gradual adhesion removal as a result of the presence of carbonitrides and porosity (compare Fig. 5e with d).

The third type of the compound layer intensive adhesive removal occurs at the crack sites, e.g., three-point cracking shown in Fig. 5f. Due to increased brittleness and lower strength at sites

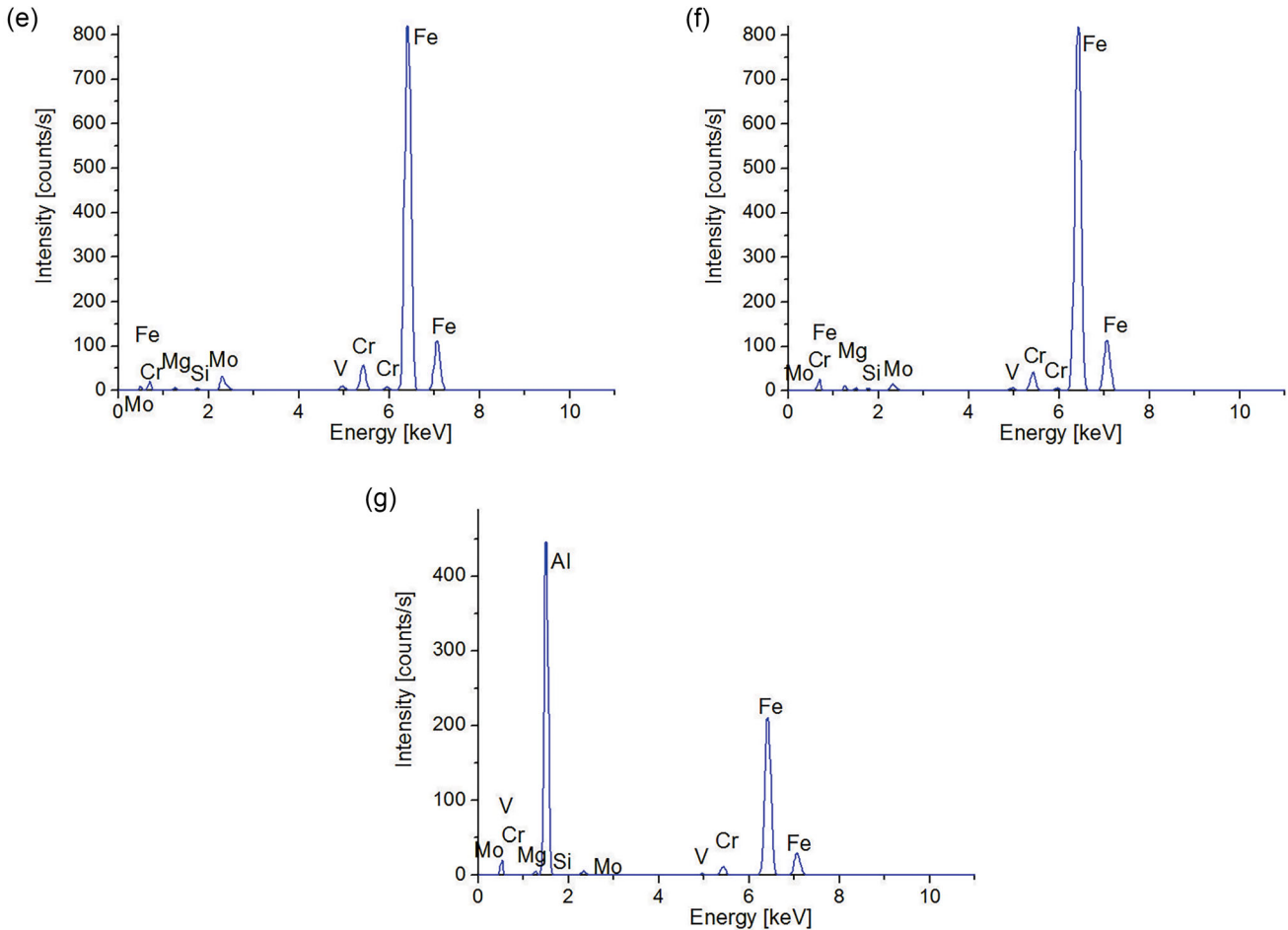


Fig. 4. continued

with increased density of carbonitrides and porosity, and in relation to the normal and frictional contact pressure (see Fig. 5f), surface cracking occurs in the compound layer. Furthermore, in Fig. 5f (right crack on the right side), the degradation of the compound layer can be observed due to the widening of the crack gaps seen as edge crumbling. Figure 5g and h clearly shows that the presence of carbonitrides and porosity is also responsible for the occurrence of cracks in the compound layer.

The different rates of adhesive removal of the compound layer can be attributed to the above-mentioned local variability of properties as well as contact pressures. A comparison of the surfaces of the specimens after 30 min and 60 min of testing (see Figs. 4 and 5) shows that a greater number of cracks in the compound layer occur in the latter, which contributes to degradation in the next stage of the wear process. Figure 5a shows that the initial surface damage, exhibited as increased roughness due to hand grinding, has no significant effect on the degradation of the compound layer.

After 2 h of testing of block 1, the following degradation processes of the compound layer were observed (Fig. 6a (SEM) and b (BSE) showing the

same area): (1) continuation of cracking in the compound layer and (2) its detachment by adhesion. Detachment by adhesion occurs both in places due to the presence of carbonitrides and porosity and in places without their visible presence. In addition, patches with signs of reactions with the hot Al were also observed. There are almost no undamaged areas on the tested surface. To show the degradation processes in more detail, areas with less damaged surfaces are shown in the following figures. Figure 6a (SEM) (see also denoted spots for details C1 in Fig. 6c and d and C2 (in Fig. 6e and b (BSE)) shows the same location on the tested surface. Detail C1 is shown in Fig. 6c and d for SEM and BSE, respectively; the removal process has progressed to the point where the beginning of fragmentary removal (tearing off) of the diffusion layer is visible. In addition to the cracking of the compound layer, which has a considerable impact on wear (detail C1 in Fig. 6c and d), visible signs of the reaction with hot Al are shown in these images (detail C2 in Fig. 6e). The cracking can be attributed to the high adhesion between the tested surface and the Al cylinder. Indeed, hot aluminum in contact with the diffusion layer tends to adhere to it, but rotation of the Al

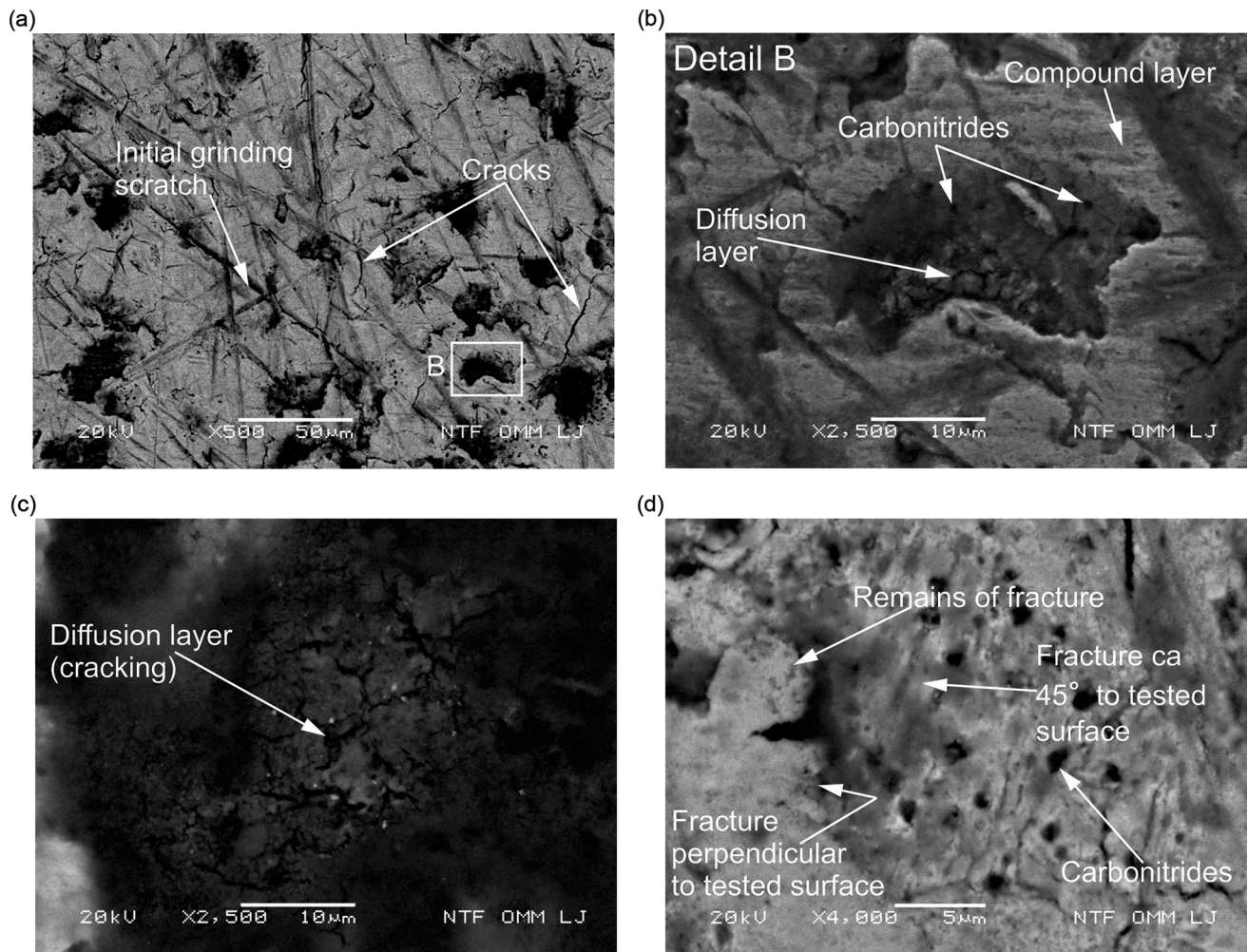


Fig. 5. Main wear characteristic of the compound layer of block 1 after 60 min of testing: (a) overall micrograph with the main damage (BSE) with marked location for detail B, (b) detail B of the formed island (BSE) marked in (a), (c) typical cracks on the underside of the islands (BSE), (d) break-off of the compound layer with visible porosity underneath (BSE), (e) shallow formed islets with porosity at the points of partial removal (BSE), (f) three-point cracks with visible porosity and widening of the crack spacing, (g) partially removed compound layer with cracks at its removal (BSE), (h) detail of initial cracking as a result of porosity (BSE); low contact pressure, sliding direction ←, block 1.

cylinder interrupts this adhesion. Repeating this process causes the surface to crack and the compound and diffusion layers to tear off. This is considered the next stage of degradation. The fragmentary tearing off indicates a sharp-edged appearance of the surface, while the spots (see Fig. 6c and d) with decreased sharpness of edges indicate a chemical reaction with hot Al. Figure 6e (detail C2) shows the next stage of the degradation process in relation to Fig. 6c and d, where clear signs of chemical attack (rounded edges on the surface) are observed in addition to cracks. The appearance of a surface with rounded edges (Fig. 6e) additionally confirms that removal of the nitrided surface is also due to reactions with hot Al. It is worth noting that at these locations (Fig. 6e), the removal of the nitrided layer also occurs based on chemical reactions as an individual wear mechanism. As is generally known, chemical reactions can also be active during bonding between the compound layer and hot Al, and consequently contribute to adhesion. However, this leads

to the tearing of small fragments from the nitrided surface and, consequently, also to the formation of sharp edges at the ablation (removal) sites (see Fig. 6c and d). From these results, it can be deduced that, in the first phase of wear progression, the predominant wear mechanism is adhesive ablation (tearing off) and not so much based on chemical reactions (i.e., chemical reactions with hot Al as an individual wear mechanism). However, these are active in bonding between hot Al and nitrided surface and they can contribute to bonding, i.e., adhesion.

Note that there are also areas on the same tested block (see Fig. 6f, see also the marked location for detail C3) where the extent of the compound layer ablation, as well as its cracking, is both more intense and less intense than in the case shown in Fig. 6a and b. Detail C3 in Fig. 6g shows that the extent of cracking is greater in areas where the compound layer has been partially removed relatively early. In the same figure (the area on the

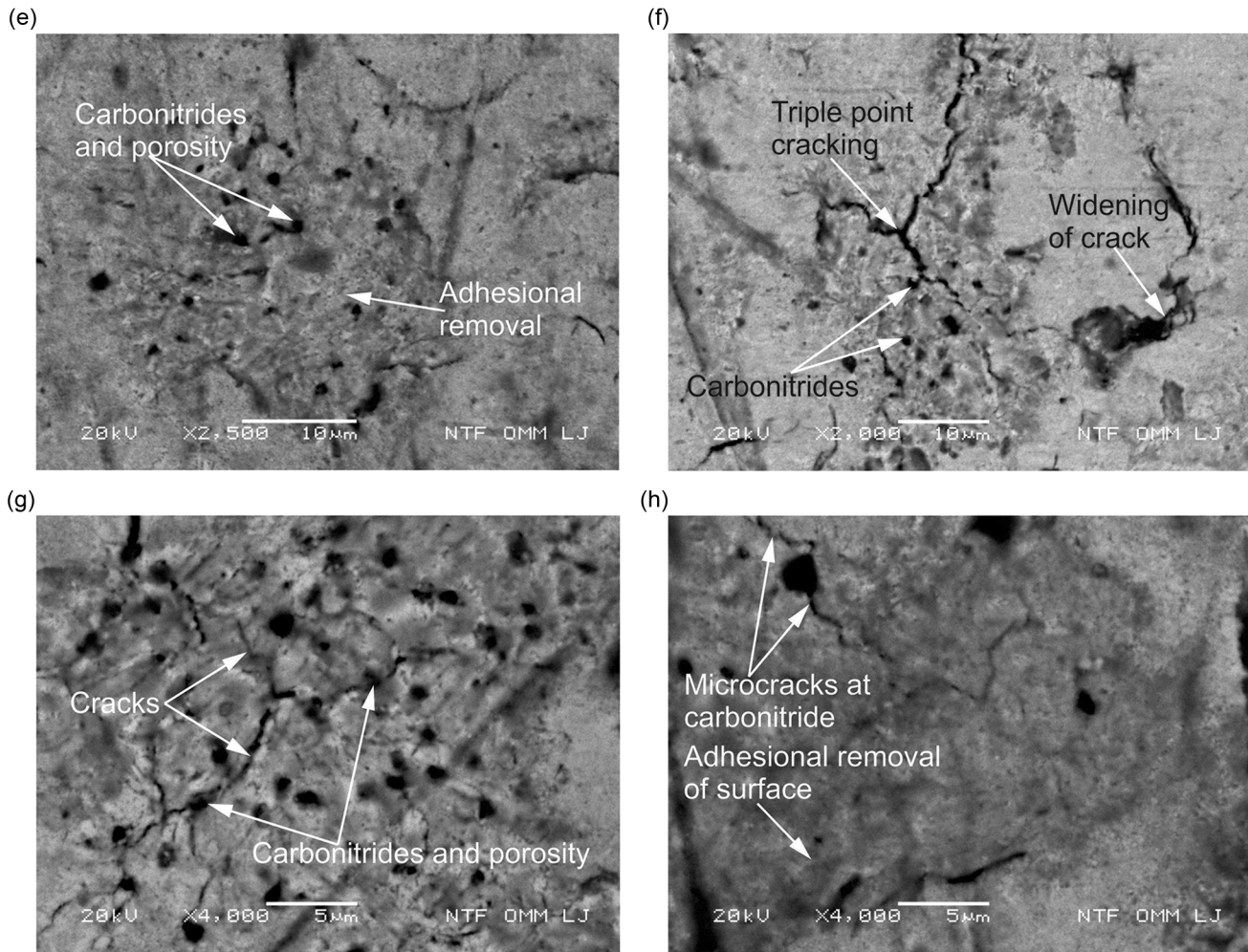


Fig. 5. continued

lower right), the crack gap begins to widen due to both the removal of edge fragments and reactions with hot Al. In addition, the edges in the transition areas from the removed to the partially removed compound layer have lower stiffness, which leads to accelerated cracking in the compound layer at these locations. Here, the cracks are oriented perpendicular to the sliding direction of the Al (see Fig. 6h).

Block 3

As already explained, blocks 3 and 4 exhibited a higher porosity density of the compound layer, a lower diffusion depth, and a lower hardness profile compared to blocks 1 and 2 indicating a potentially poorer resistance to degradation. Examination of the microstructure (nitriding depth, compound layer thickness, presence of carbonitrides and porosity, etc.) of blocks 3 and 4 revealed that the compound layer may have different properties (slightly worse) compared to blocks 1 and 2, which may influence the progress of degradation. Similar degradation progress was also observed, for example, in block 3, which was tested with the same

contact pressure as block 1, but at a higher rate. The typical appearance of the tested surface after 30 min of testing is shown in Fig. 7a (SEM, see also the highlighted point for detail D1). Detail D1 can be seen in Fig. 7b (SEM), where the adhesional removal due to carbonitrides (see remains of the bottom of islet) and porosity is again visible (similar to Figs. 5 and 6). The increased adhesive removal on block 3 after 60 min of testing results in the typical surface appearance shown in Fig. 7c (SEM, see the location shown in Fig. 7d for detail D2), where the formation of craters with a size of 30–40 μm is visible. In some places, the first signs of directional erosion (in sliding direction-oriented removal) were also observed (see Fig. 7d). The EDS analysis (see marked locations in Fig. 7c) was carried out at site 1, where the compound layer is almost undamaged, and at site 2, where the compound layer has been completely removed. EDS again showed the presence of Al and Mg at site 2, indicating a chemical reaction with hot Al, while no Al and Mg were detected at site 1. After 2 h of testing, increased evidence of furrow formation was observed, due to the connection of several distant islands in the

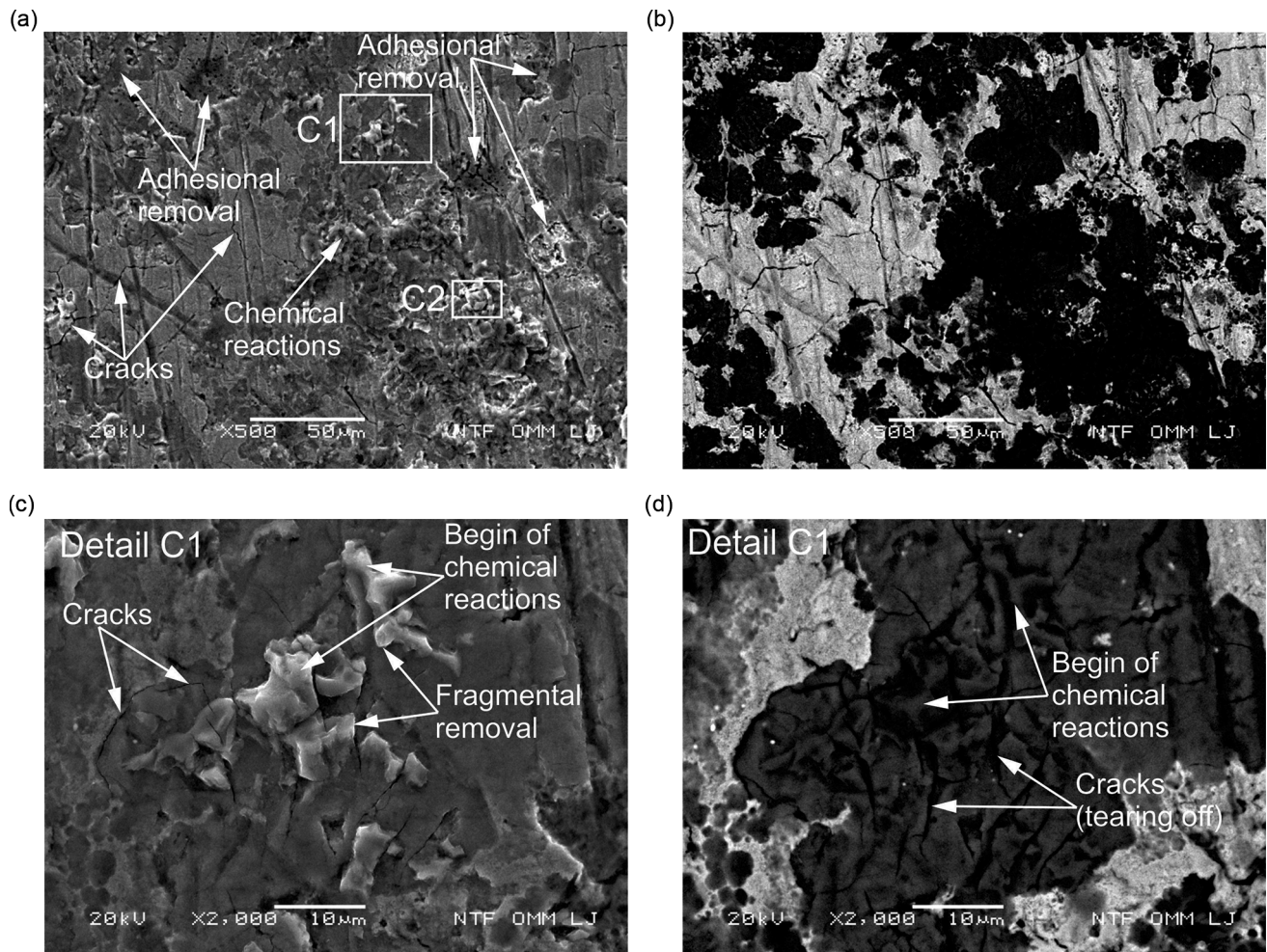


Fig. 6. Main wear characteristic of the tested nitrided surface layer of block 1 after 120 min of testing: (a) appearance of the tested surface (SEM) with marked locations for details C1 and C2, (b) appearance of tested surface (BSE), (c) detail C1 of fragmentary removal of less damaged tested surface (SEM), (d) detail C1 of fragmentary ablation of less damaged tested surface (BSE), (e) detail B of fragmentary ablation with chemical attack of more damaged tested surface (BSE), (f) less damaged area of the tested surface with marked location for detail C3 (BSE), (g) detail C3 of the extension of the cracks from the area of the diffusion layer to the area with the remaining compound layer and widening of the crack (BSE, right side), (h), partial removal of the compound layer with the appearance of a crack oriented perpendicular to the sliding direction (BSE); low contact pressure, sliding direction ←, block 1.

sliding direction, as shown in Fig. 7e (SEM) with the location for detail D3 shown in Fig. 7f. This stage is related to the initial furrow formation normally observed on the bearing surface of extrusion dies when they are to be adjusted to a new grinding-nitriding cycle (the final stage of furrow formation at the die-bearing surface is shown in Fig. 1d).

Wear Progress at Medium (M) Contact Pressures

The wear process at medium contact pressure was tested on blocks 2 and 4 and the progress of degradation is described below.

Block 2

As shown above in the low contact pressure tests, block 1 generally has better compound layer properties (see Figs. 2 and 3) compared to block 3, as it

has a lower rate of degradation. This is also true for block 2 compared to block 4 in medium contact pressure tests. Adhesion detachment after 30 min and 60 min (see Fig. 8a (SEM) with the location shown in Fig. 8b (SEM) for detail E1) is predominant, but with a higher density compared to block 1 (see Figs. 4 and 5 for low contact pressures) and only small surface cracks were observed. Figure 8b shows that the islands removed by adhesion are increased at sites with higher carbonitride density and porosity compared to sites where this is not as pronounced.

In testing up to 120 min, the islets (areas) removed by adhesion increase and the first signs of oriented removal in the sliding direction are observed, as can be seen in Fig. 8c (SEM), where the location for detail E2 shown in Fig. 8d (SEM) can also be seen. It should also be emphasized here that, due to the increase in area and depth of the removed

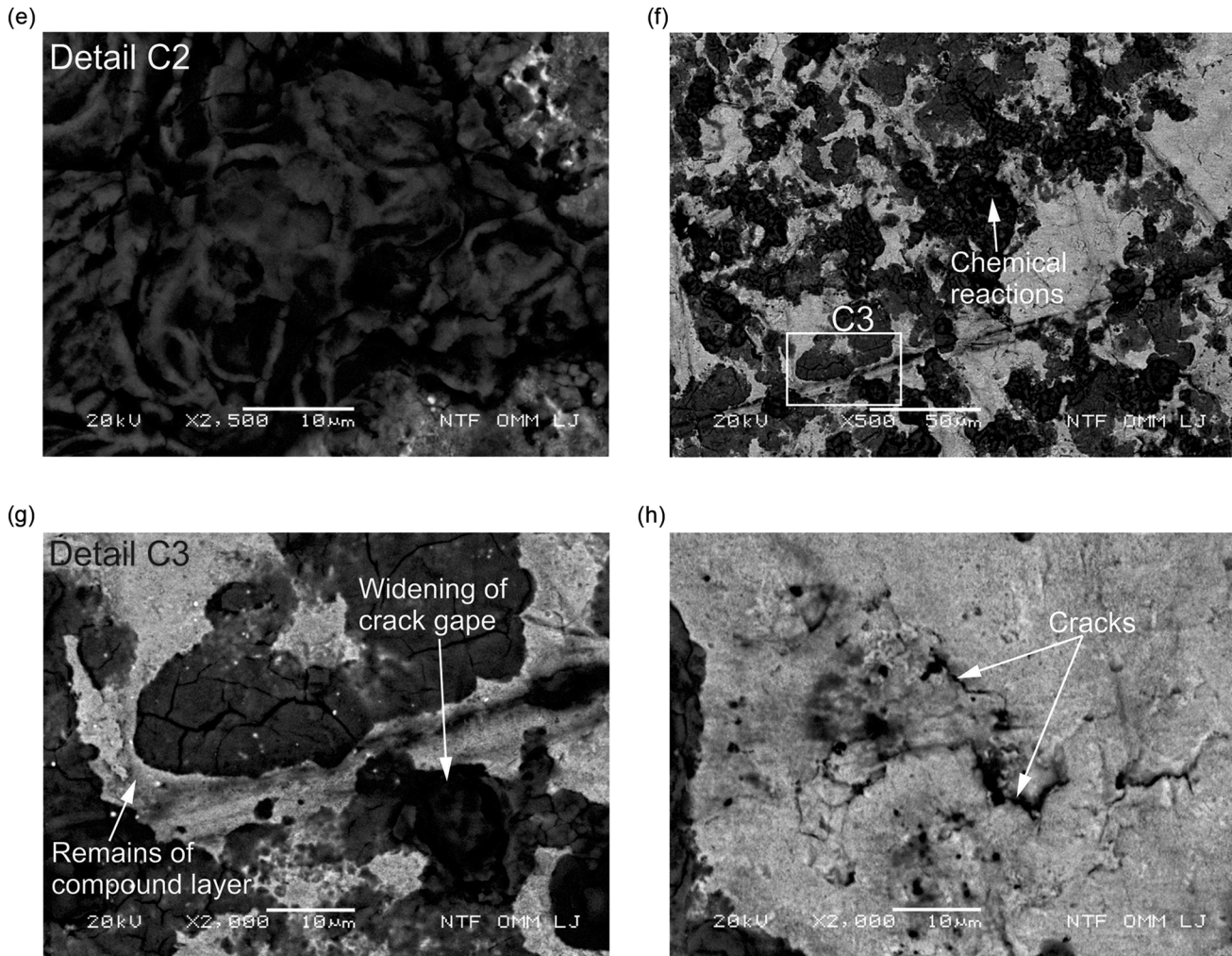


Fig. 6. continued

islets during the test, there is a weakening of the wall thickness between the removed islets, which leads to a deformation or tear-off of the walls between them in the sliding direction. This is the first step in the formation of furrows.

The main difference in the surface appearance testing at low and medium contact pressures is the increased density of the adhesion sites. This means that the formation of furrows generally takes place earlier at testing with medium contact pressure. On the other hand, less cracking as well as sites with hot Al reaction were seen. However, this does not mean that the mentioned processes do not take place. This can be attributed to increased adhesion leading to earlier detachment of the adhesion at weak points, although small cracks or chemical reactions have occurred before.

Block 4

The typical appearance of the tested surface of block 4 after 30 min of testing is shown in Fig. 9a (SEM), where the area of detail F1 is marked. The degradation of the compound layer for block 4 is

more intense in spots of increased carbonitride density and porosity, where adhesive removal is more pronounced (see detail F1 in Fig. 9b). Adhesion erosion was also observed at locations where almost no carbonitrides and porosity were observed at the adhesion sites (see denoted area F2 in Fig. 9b) which is attributed to a higher amount of oxygen on the top of the compound layer (see Fig. 2). When tested for up to 60 min, the wear process continues and can be observed as an increased density of islets of the removed compound layer with relatively thick walls between the islets, as shown in Fig. 9c (see also highlighted area for detail F3). The increased density of the removed islets is a result of the occurrence of increased frictional stresses as well as the previously increased microcracks. Figure 9d (SEM) shows a detail F3 where a larger adhesive removal (ablation) area of about 50 μm is visible. Other small areas removed by adhesion (i.e., islets with decreased depth and size) are visible nearby where there is less presence of carbonitrides and porosity. Figure 9e (SEM) shows several locations where the areas previously removed by adhesion are

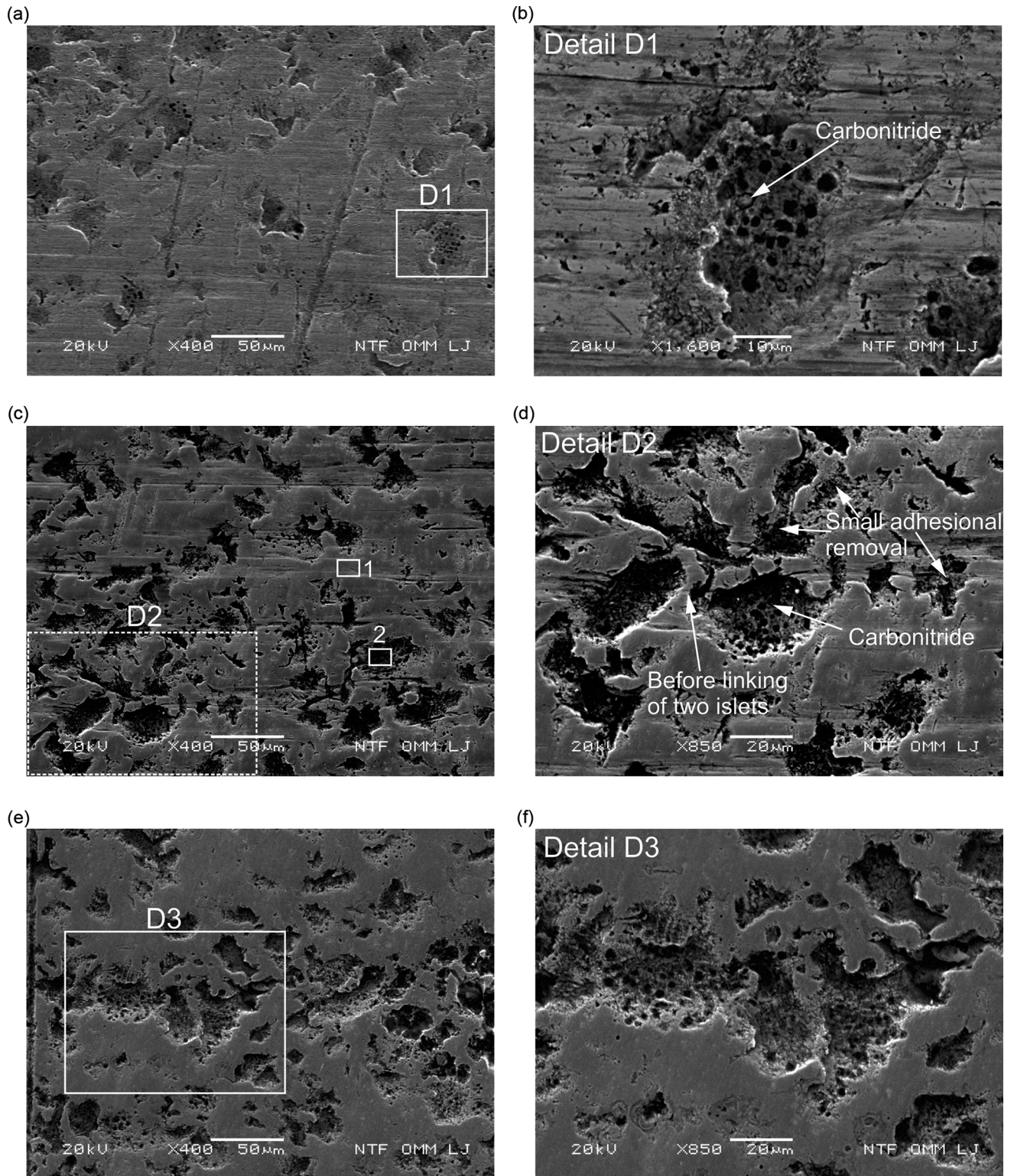


Fig. 7. Main wear characteristics of the tested nitrided surface layer of block 3, after 30-min test (SEM) with location marked for detail D1: (a) adhesion removal at locations with porosity present, (b) detail D1, presence of porosity at locations removed (SEM), (c) after 60-min test with location marked for detail D2, (c) increasing size and density of islands removed by adhesion, (d) detail D2, (e), after 120-min test with site indicated for detail D3, (e) first signs of removal in sliding direction (SEM), (f) in detail D3; low contact pressure, sliding direction ←, block 3.

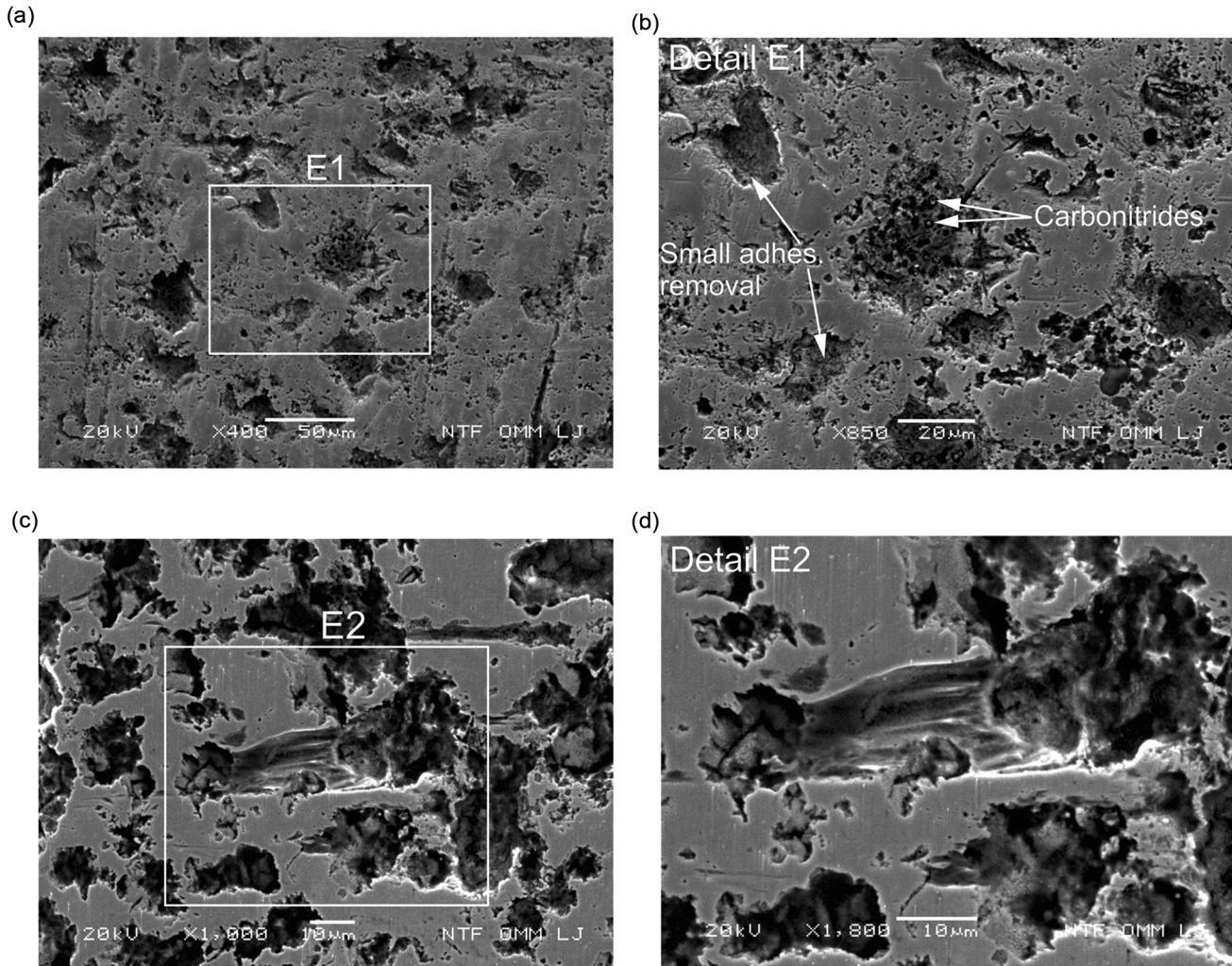


Fig. 8. Main wear characteristics of tested surface of block 2: (a) after 60-min test with marked location for detail E1, (b) detail E1 shows adhesion erosion at locations of increased carbonitride density and porosity (BSE), (c) after 120-min test with marked location for detail E2, (d), detail E2 shows deformation of wall between removed islands (BSE); tested at medium contact pressure, direction of sliding \leftarrow , block 2.

combined with presence of carbonitrides and porosity. The figure also shows the location for detail F4 in Fig. 9f, where the joining of three areas of increased carbonitrides and porosity can be seen. Figure 9e also shows an area (labeled F5) where the increased density of the removed areas can be seen where carbonitrides and porosity are not present.

As mentioned earlier, areas of varying degrees of wear progress were observed. Figure 10a (SEM), for example, shows a more damaged area with significant furrowing in the direction of sliding. Such areas of wear progression most likely relate to the previous stage of damaged areas, as shown in Fig. 9e and f (medium contact pressure test and 60 min of testing). In addition, after 120 min of testing, areas with an increased density of islets of the removed compound layer with relatively thick walls between the islets were observed, as shown in Fig. 10b (BSE). The increased density of removed islets is a result of the occurrence of increased

frictional stresses. Typical G1 and G2 details can be seen in Fig. 10c (SEM) and d (SEM), with almost no carbonitrides and porosity, but clearly visible cracks on the underside of the islets. This may be the result of increased adhesive (fragmentary) removal, even in areas where the density of carbonitrides and porosity is lower. In addition, areas where adhesion was not as intense were also observed, as detachment is not so much due to the presence of carbonitrides and porosity (as also shown in Fig. 9b), which means that adhesion detachment occurs is predominantly small sized. This is illustrated in Fig. 10e (SEM), where a larger area of such adhesion detachment can be seen. Detail G3 of the typical appearance at the ablation site is shown in Fig. 10f (SEM), where a limited area of porosity is shown in conjunction with an area of almost no carbonitrides and porosity. This variation in wear progression can be attributed to both variation in the properties of the nitrated layer and the

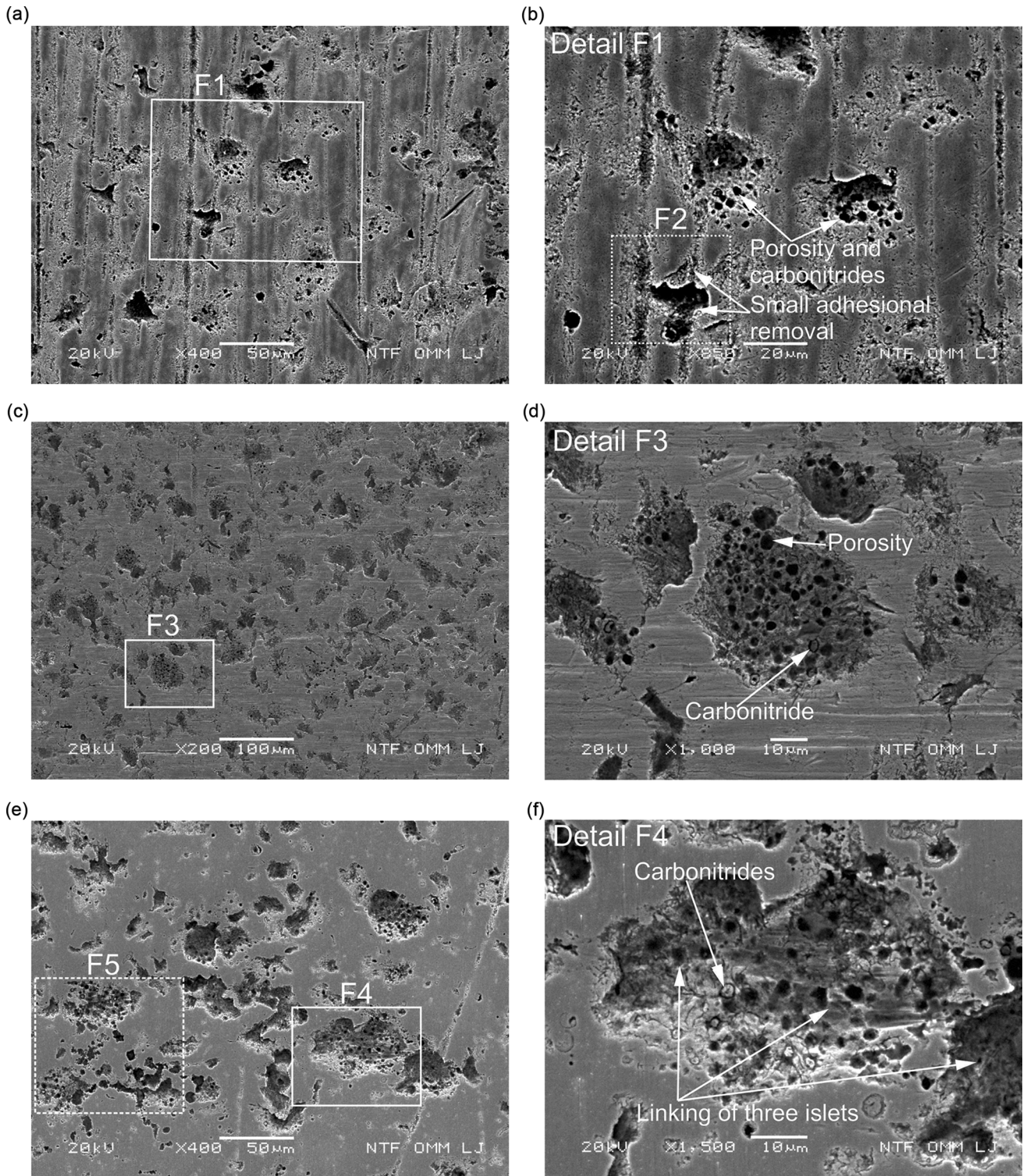


Fig. 9. (a, b) Main characteristics of wear on the tested surface of block 4 after 30 min and (c–f) 60 min of testing: (a) adhesion wear on the base of the compound layer due to the presence of carbonitrides and porosity with marked location for detail F1, (b) detail F1 shows areas of low adhesion wear and increased adhesion wear on the location with presence of carbonitrides and porosity and low adhesion wear on location F2, (c) increased density and size of areas of adhesion erosion with marked location for detail F3, (d) detail F3 with areas of low adhesion erosion and increased adhesion erosion at a location with dense carbonitrides and porosity, (e) linkage of multiple areas of adhesion erosion at locations with dense carbonitrides and porosity with marked location for detail F4 and area F5, (f) detail F4 with linkage (SEM); medium contact pressure, sliding direction ←, block 4.

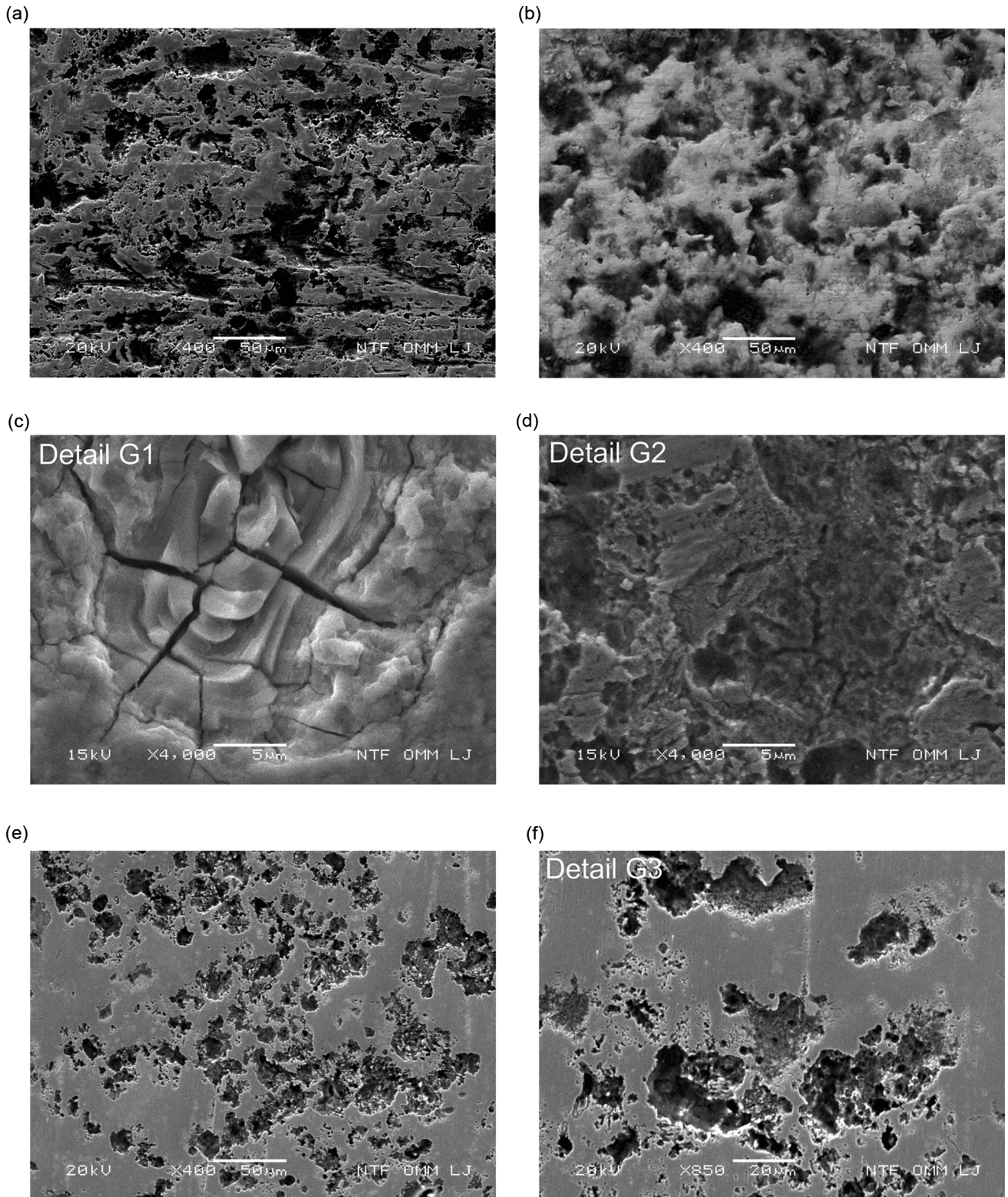


Fig. 10. (a) Main wear characteristic of the tested surface of block 4 after 120 min of testing; formation of furrows oriented in the direction of sliding (SEM), (b) increased density of adhesive abrasion (BSE), and (c, d) typical detail G1 and detail G2 of the ablated islets with cracking at the sites of adhesive abrasion (SEM), (e) adhesive abrasion in the area with reduced occurrence of carbonitrides and porosity (SEM), (f) with typical detail G3; medium contact pressure, sliding direction \leftarrow , block 4.

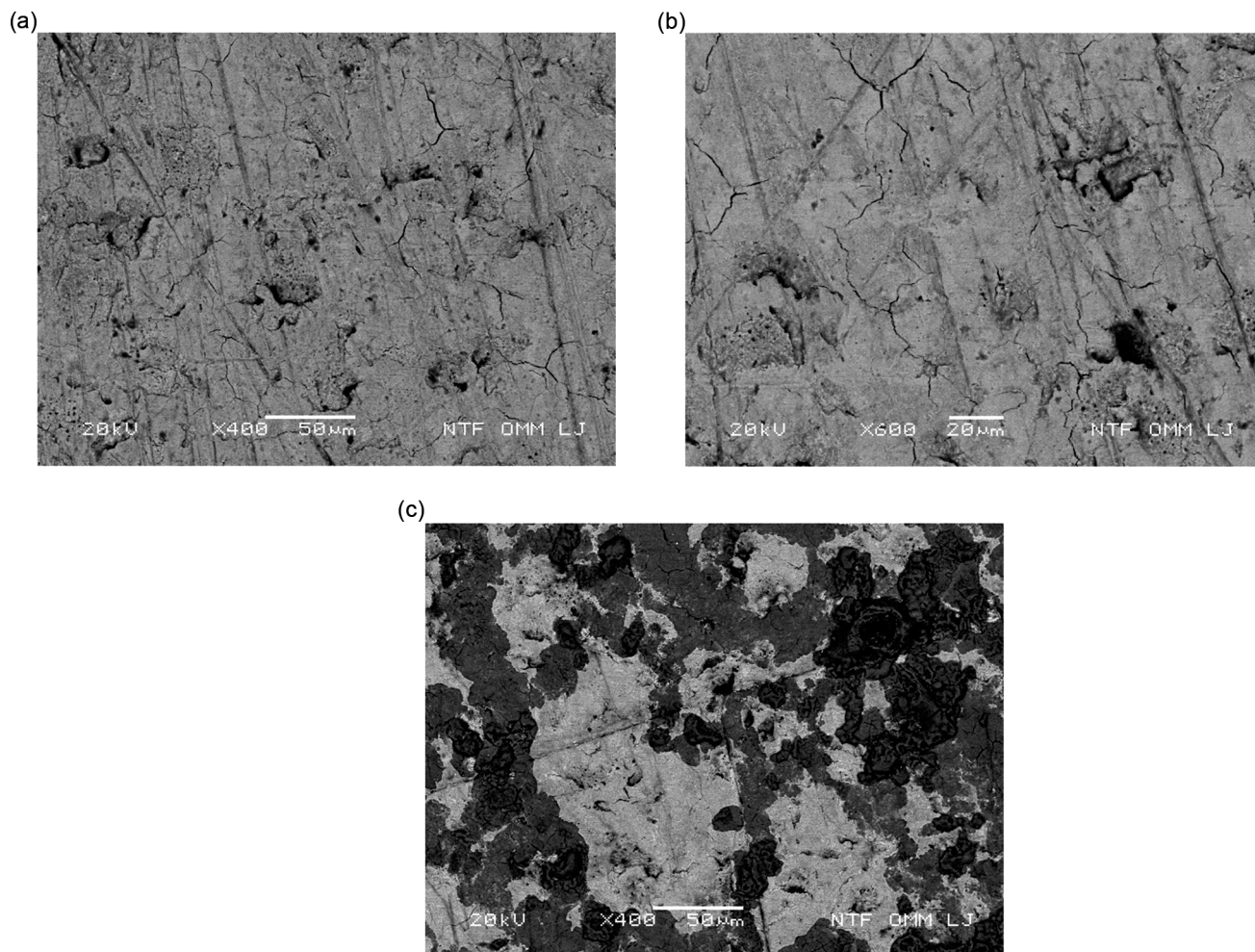


Fig. 11. Appearance of the surface in the area of the lower contact pressures (see Fig. 1b) after 120 min of testing on block 1 (BSE): (a) small cracks and adhesion detachment, (b) detail H1, (c) chemical reaction with hot Al; lower contact pressures, sliding direction ←, block 1.

prevailing contact pressures. As mentioned, the contact pressures are not the same along the entire contact length, i.e. even in the area with higher contact pressures, as shown schematically in Fig. 1b. It is assumed that there is a slight decrease towards the area with lower contact pressure.

Wear Progress at Lower (LR) Contact Pressures

In the area of the surface tribologically stressed by lower contact pressures (see Fig. 1b), blocks 1 and 3 were only analyzed after 120 min of testing. Despite significantly lower contact pressures in the surface compared to the surface with higher contact pressures, differences in wear progress were also observed on the surface.

Block 1

The main features for the tested area with lower (LR) contact pressure after 120 min of testing on block 1 are thus predominantly surface cracks as

well as small adhesive removal of the compound layer, as shown in Fig. 11a and in detail H1 in Fig. 11b, where the extent of wear progress is significantly lower compared to the area with low (L) contact pressure. The two aforementioned sites of surface damage are also potential sites for chemical reactions, which can be seen at a more pronounced stage depicted in Fig. 11c. The figure clearly shows the onset of chemical reactions at the sites of compound layer removal. Variations in the extent of chemical reaction were also observed in this area (i.e., at lower (LR) contact pressure), but on the left side of the area (see Fig. 1b), where there is presumably the lowest contact pressure, the least progress in degradation was also observed (Fig. 11a and b).

Thus, in the area where lower contact pressure prevails, the adhesion removal is also lower, allowing the wear to progress based on the chemical reaction as individual wear mechanism. The wear rate in this case is lower than in the cases where adhesive removal predominates.

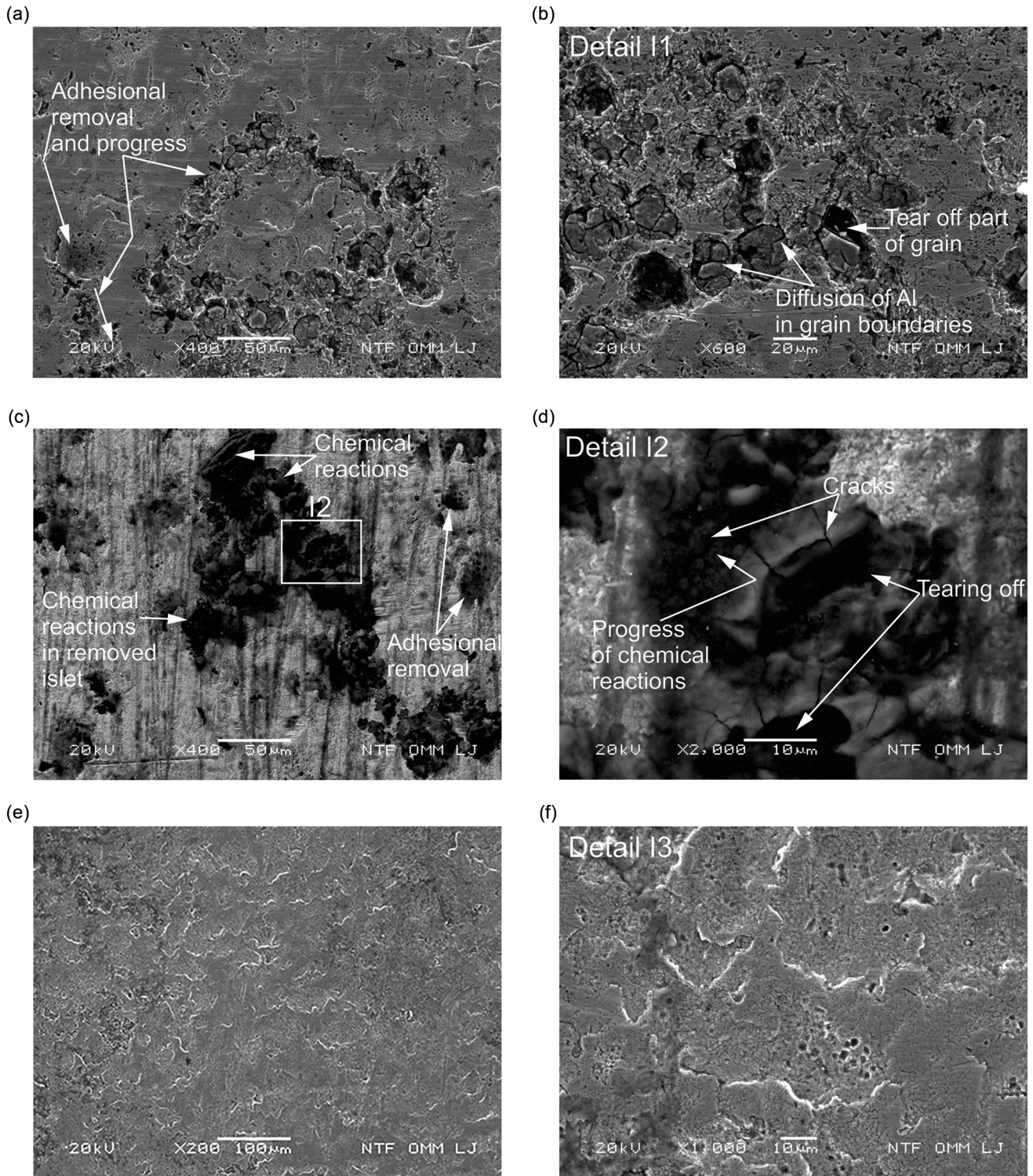


Fig. 12. Appearance of the surface with lower contact pressure after 120 min of testing on block 3; (a) area of adhesion removal with chemical reactions on the surface (SEM), (b) detail I1 showing removal of particle grains on the surface at the sites of adhesion removal due to diffusion of Al in the grain boundaries (SEM), (c) location of chemical reactions with hot Al starting at the site of previous adhesion removal and designated site for detail I2 (BSE), (d) detail I2 showing the adhesion removal of the chemically attacked area as well as the progress of chemical reactions in the surrounding area (BSE), (e) very shallow adhesion removal in the area of the very low contact pressures (SEM), (f) showing detail I3 (SEM); lower contact pressures, sliding direction ←, block 3.

Block 3

The density of adhesive removal was low and almost no cracking was observed. Figure 12a (SEM) shows the area with adhesive removal of the compound layer, with a typical detail I shown in Fig. 12b (SEM). In the last figure, the appearance of cracks in the diffusion layer can be seen, partly due to the diffusion of Al in the grain boundaries, as well as cracking in the surface area of the grains due to fatigue (sticking and separation) and frictional loading of the surface. Further on, the figure shows both patches with partially removed surface grains and patches with completely removed parts of surface grains of the diffusion layer. In Fig. 12c (BSE, see also the location for detail I2), there are patches of adhesive removal as well as an area where reactions with hot Al took place. The reaction with hot Al started at the site of the previous adhesion removal. The state of the chemical reactions in progress is shown in detail I2 in Fig. 12d (BSE), where the removal of the surface layer at the site of the previous chemical reactions and the progress of the chemical activity in the vicinity are clearly visible. Due to the increase in volume after the chemical reaction, cracking and adhesive removal are also visible. As mentioned earlier, hardly any cracks were visible in the compound layer in the area. In Fig. 12e (SEM), which refers to the left part of the area (i.e., the very low (VL) contact pressures (cf. Fig. 1b), only minor adhesion removal is visible in detail I3 shown in Fig. 12f (SEM).

The reactions with the hot Al as individual wear mechanisms were observed predominantly at lower contact pressures in both microstructures, i.e., blocks 1 and 3. Thus, in tests with lower contact pressure, this was observed in block 1, where adhesion removal was less pronounced, while in block 3, with increased adhesion removal, this extent was slightly higher. Adhesion sites also serve as triggers for reactions with the hot Al. At low contact pressure, the reactions were more pronounced at block 1, despite their limited low extent, because the adhesive removal was lower compared to block 3, so the adhesive removal of chemically attacked areas could also be detected at some smaller locations. This was not observed at medium contact pressure (i.e., blocks 2 and 4) with increased adhesive removal.

This does not mean that the reaction with hot Al as an individual wear mechanism is not also active in such cases, i.e. under conditions of increased adhesion removal. Under conditions of strong adhesion, such areas that have been subjected to chemical reactions are removed at an early stage of the process of chemical reactions and therefore this behavior is hardly noticeable at the previously selected times of test interruption. Reactions are of course also active in the bonding between the hot Al and the nitrided surface layer resulting in adhesive

removal and in such cases reactions cannot be considered as an individual wear mechanism.

CONCLUSION

A laboratory wear test rig "block on hot Al cylinder" was used to investigate the degradation processes of two different qualities of the nitrided layer of H10 tool steel, taking into account the occurrence of contact pressures between the tested block and the hot Al, i.e., their distribution along the specified contact length. Considering the wear behavior, the established contact length (zone) between the hot Al cylinder and the tested block was conditionally and roughly divided into two areas during the test with low contact pressures, i.e., an area with low and an area with lower contact pressures. Four blocks were gas nitrided and surface oxidation followed gas nitriding. Two different properties of the compound layers were obtained, which were tested for their wear behavior. Considering the wear progress on the tested blocks, the tests were performed at lower, low, and medium contact pressure. The following conclusions can be drawn regarding the tested properties of the compound layers with respect to the contact pressure used and wear behavior of the compound and diffusion layers:

1. In the gas nitriding process, compound layers were obtained consisting predominantly of the ϵ -phase. The presence of carbonitrides and porosity was observed in the compound layer. Two different characteristics in terms of oxidation, thickness, and the presence of carbonitrides and porosity were tested for wear behavior.
2. In blocks 1 and 2, the presence of oxygen in the surface layer of the compound layer was weak, while it was more pronounced in blocks 3 and 4. The presence of carbonitrides and porosity was observed in both compound layers, which were not uniformly distributed. A random distribution of their increased density was observed at sites of adhesive removal.
3. Adhesive erosion (removal), cracking, and chemical reactions with hot Al are the main wear mechanisms. Their contribution to the wear processes depends on the density of the presence of carbonitrides, porosity, and oxygen and is related to the contact pressures. The wear rate increases with increasing contact pressure and with increasing presence of carbonitrides and porosity in the compound layer. Differences in wear rate were found depending on the properties of the compound layer and the contact pressure.
4. Chemical reactions as an individual wear mechanism are more pronounced at lower contact pressures, with less adhesive erosion compared to low and medium contact pressures.

5. The diffusion layer is more susceptible to earlier reactions with hot Al due to its lower N content compared to the compound layer.
6. Locations of adhesive removal and gap between cracks can serve to initiate reactions with hot Al. Adhesive removal at these sites was also observed, as the brittleness was increased, facilitating crack formation and consequently adhesion removal.
7. Adhesion was more pronounced with less cracking in the compound layer.
8. Thickness of the compound layer, nitriding depth, hardness profile, properties of the compound layer, and contact pressure should be considered as an integral part of the wear processes. Wear behavior is very complex. The applied contact pressure and the integral properties of the nitriding play a decisive role in determining the degradation paths and the wear rate, i.e., for the time of occurrence of the typical degradation phase, adhesive removal and cratering, cracking in the compound layer, cracking in the diffusion layer, and adhesive removal in the sliding direction.
9. The formation of furrows observed as removal of the nitrided layer in the sliding direction is the final stage of the degradation process. It depends on the contact pressure applied, the quality of the tested surface layer, and the rate of adhesive removal. Furrows appear earlier when test pressure is increased.
10. It is possible to increase the die life by improving the properties of the nitrided layer and by reducing the contact pressures on the bearing surface through improved die design.

CONFLICT OF INTEREST

The authors declare that they have no conflict of interest.

OPEN ACCESS

This article is licensed under a Creative Commons Attribution 4.0 International License, which permits use, sharing, adaptation, distribution and reproduction in any medium or format, as long as you give appropriate credit to the original author(s) and the source, provide a link to the Creative Commons licence, and indicate if changes were made. The images or other third party material in this article are included in the article's Creative Commons licence, unless indicated otherwise in a credit line to the material. If material is not included in the article's Creative Commons licence and your intended use is not permitted by statutory regulation or exceeds the permitted use, you will need to obtain permission directly from the copyright holder. To view a copy of this licence, visit <http://creativecommons.org/licenses/by/4.0/>.

REFERENCES

1. A. Berrais, A. Boudebane, M. Labaiz, A. Montagne, S. Lemboub, M.Z. Touhami, and A. Ourdjini, *Wear* 514–515, 204587 <https://doi.org/10.1016/j.wear.2022.204587> (2023).
2. A.F.M. Arif, *Mater. Manuf. Process.* 24, 619 (2009).
3. P. Matteis, G. Scavino, E. Quadrini, P. Perucci, and D. Firrao, *Surf. Eng.* 25(7), 507 (2009).
4. T. Björk, R. Westergård, and S. Hogmark, *Wear* 249, 316 (2001).
5. Y. Birol, *Eng. Fail. Anal.* 26, 203 (2012).
6. Y. Birol and B. Yuksel, *Surf. Coat. Technol.* 207, 461 (2012).
7. M. Pellizzari, M. Zadra, and A. Molinari, *Surf. Eng.* 23(3), 165 (2007).
8. P. Panjan, P. Cvahte, M. Čekada, B. Navinšek, and I. Urankar, *Vacuum* 61, 241 (2011).
9. N.D. CamposNeto, A.L. Korenyi-Both, C. Vian, S.P. Midson, and M.J. Kaufman, *J. Mater. Process. Technol.* 316, 117954 <https://doi.org/10.1016/j.jmatprotec.2023.117954> (2023).
10. Y. Birol, *Tribol. Int.* 57, 101 (2013).
11. M. Pellizzari, *Wear* 271, 2089 (2011).
12. K.B. Müller, *J. Mater. Process. Technol.* 130–131, 432 (2002).
13. K.E. Cooke, S. Yang, C. Seluck, A. Kennedy, D.G. Teer, and D. Beale, *Surf. Coat. Technol.* 188–189, 697 (2004).
14. G. Wang, B. Cui, W. Zou, X. Xiong, Y. Pan, F. Liu, M. Zhou, G. He, H. Chen, and S. Qu, *Int. J. Fatigue* 157, 106725 <https://doi.org/10.1016/j.ijfatigue.2022.106725> (2022).
15. M. Kaba, M. Altay, E. Akyildiz, F. Muhaffel, S. Ozkurt, E. Atar, M. Baydogan, and H. Cimenoglu, *Wear* 498–499, 204300 <https://doi.org/10.1016/j.wear.2022.204300> (2022).
16. B. Wang, X. Zhao, W. Li, M. Qin, and J. Gu, *Appl. Surf. Sci.* 431, 39 (2018).
17. T. Mori, N. Takatsuji, K. Matsuki, T. Aida, K. Murotani, and K. Uetoko, *J. Mater. Process. Technol.* 130–131, 421 (2002).
18. M. Terčelj, G. Kugler, R. Turk, P. Cvahte, and P. Fajfar, *Int. J. Veh. Des.* 39(1–2), 93 (2005).
19. P. Psyllaki, G. Kefalonikas, G. Pantazopoulos, S. Antoniou, and J. Sideris, *Surf. Coat. Technol.* 162, 67 (2002).
20. M. Hernandez, M.H. Staia, and E.S. Puchi-Cabrera, *Surf. Coat. Technol.* 202, 1935 (2008).
21. J. Walkowicz, J. Smolik, and J. Tacikowski, *Surf. Coat. Technol.* 116–119, 70 (1999).
22. S.S. Akhtar, A.F.M. Arif, and B.S. Yilbas, *Int. J. Adv. Manuf. Technol.* 47, 687 (2010).
23. E.J. Miola, S.D. de Souza, and M. Olzon-Dionysio, *Surf. Coat. Technol.* 167, 33–40 (2003).
24. Y. Duan, S. Qu, S. Jia, and X. Li, *Wear* 464–465, 203548 <https://doi.org/10.1016/j.wear.2020.203548> (2021).
25. M.A.J. Somers and E.J. Mittemeijer, *HTM* 47, 3 <https://doi.org/10.1515/htm-1992-470313> (1992).
26. D. Lidtke, U. Baudis, J. Bosslet, U. Huchel, H. Klümper-Westkamp, W. Leche, and H.J. Spies, *Warmebehandlung von Werkstoffen, Nitrieren und nitrocarburieren*, ISBN 3-8169-2416-6 (Expert Verlag, 2006).
27. G. Castro, A. Fernández-Vicente, and J. Cid, *Wear* 263, 1375 (2007).
28. P.F. Friehling, F.W. Poulsen, and M.A.J. Somers, *Z. Metallkd.* 92(6), 589 (2001).
29. A. Molinari, U.M. Pellizzari, G. Straffelini, and M. Pirovano, *Surf. Coat. Technol.* 126, 31 (2000).
30. D.C. Wen, *Appl. Surf. Sci.* 256, 797 (2009).
31. S.-H. Chang, T.-P. Tang, Y.-C. Chen, and J.-K. Chen, *ISIJ Int.* 49(3), 421 (2009).
32. R.L.O. Basso, R.J. Candal, C.A. Figueroa, D. Wisnivesky, and F. Alvarez, *Surf. Coat. Technol.* 203, 1293 (2009).
33. D.C. Wen, *ISIJ Int.* 49(11), 1762 (2009).
34. D.C. Wen, *Wear* 268, 629 (2010).
35. D. Kundalkar, M. Mavalankar, and A. Tewari, *Mater. Sci. Eng.* A651, 391 <https://doi.org/10.1016/j.msea.2015.10.007> (2016).
36. M. Vilaseca, S. Molasa, and D. Casellasa, *Wear* 272, 105 (2011).

37. M. Terčelj, A. Smolej, P. Fajfar, and R. Turk, *Tribol. Int.* 40, 374 (2007).
38. M. Terčelj and G. Kugler, *Wear* 376–377, 1779 <https://doi.org/10.1016/j.wear.2017.01.086> (2017).
39. D. Bombač, M. Terčelj, I. Peruš, and P. Fajfar, *Wear* 307, 10 <https://doi.org/10.1016/j.wear.2013.08.015> (2013).
40. S.C. Lim and M.F. Ashby, *Acta Metall. Mater.* 24(5), 805 (1990).
41. H. So, H.M. Chen, and L.W. Chen, *Wear* 265, 1142 (2008).
42. L. Wang, Y. He, J. Zhou, and J. Duszczek, *Tribol. Int.* 43, 299 (2010).
43. L. Wang, J. Zhou, J. Duszczek, and L. Katgerman, *Tribol. Int.* 56, 89 (2012).
44. L. Wang and H. Yang, *Tribol. Int.* 56, 99 (2012).
45. X. Ma, M.B. de Rooij, and D.J. Schipper, *Wear* 278–279, 1 (2012).
46. L. Wang, J. Zhou, J. Duszczek, and L. Katgerman, *Tribol. Int.* 50, 66 (2012).
47. H.-J. Kim, A. Emge, S. Karthikeyan, and D.A. Rigney, *Wear* 259, 501 (2005).
48. F.A.P. Fernandes, S.C. Heck, C.A. Picone, and L.C. Castelletti, *Surf. Coat. Technol.* 381, 125216 <https://doi.org/10.1016/j.surfcoat.2019.125216> (2020).
49. G. Zhang, H. Cui, H. Zhang, and G. Cheng, *Tribol. Int.* 120, 226 <https://doi.org/10.1016/j.triboint.2017.12.028> (2018).
50. M. Pérez and F.J. Belzunce, *Surf. Coat. Technol.* 305, 146 <https://doi.org/10.1016/j.surfcoat.2016.08.003> (2016).
51. A.K. Gonzalez-Moran, M. Naeem, H.M. Hdz-García, E.E. Granda-Gutiérrez, J.J. Ruz-Mondragón, M. Alvarez-Vera, and J.C. Díaz-Guillén, *J. Mater. Res. Technol.* 25, 4139 <https://doi.org/10.1016/j.jmrt.2023.06.221> (2023).
52. J. Ratajski, *Surf. Coat. Technol.* 203, 2300 <https://doi.org/10.1016/j.surfcoat.2009.02.021> (2009).
53. B. Liu, B. Wang, X. Yang, X. Zhao, M. Qin, and J. Gu, *Appl. Surf. Sci.* 483, 45 <https://doi.org/10.1016/j.apsusc.2019.03.291> (2019).
54. P. Cavaliere, A. Perrone, and A. Silvello, *Eng. Sci. Technol. Int. J.* 19, 292 <https://doi.org/10.1016/j.jestch.2015.07.004> (2016).
55. I. Bedii Ozdemir and F. Akar, *Vacuum* 116, 104 <https://doi.org/10.1016/j.vacuum.2015.03.004> (2015).
56. H. Aghajani, M. Torshizi, and M. Soltanieh, *Vacuum* 141, 97 <https://doi.org/10.1016/j.vacuum.2017.03.032> (2017).
57. Y. Birol, *Surf. Coat. Technol.* 205, 2763 <https://doi.org/10.1016/j.surfcoat.2010.10.044> (2011).
58. Z. Gronostajski, P. Widomski, M. Kaszub, M. Zwierzchowski, S. Polak, Ł. Piechowicz, J. Kowalska, and M. Długozim, *J. Manuf. Process.* 52, 247 <https://doi.org/10.1016/j.jmapro.2020.01.037> (2020).
59. J. Miyamoto and P. Abraha, *Surf. Coat. Technol.* 375, 15 <https://doi.org/10.1016/j.surfcoat.2019.07.001> (2019).
60. J. Peng, Z. Zhu, and D. Su, *Tribol. Int.* 129, 232 <https://doi.org/10.1016/j.triboint.2018.08.017> (2019).
61. Y. Ren, P. Wang, Z. Cai, J. He, J. Lu, J. Peng, X. Xu, and M. Zhu, *Tribol. Int.* 170, 107496 <https://doi.org/10.1016/j.triboint.2022.107496> (2022).

Publisher’s Note Springer Nature remains neutral with regard to jurisdictional claims in published maps and institutional affiliations.